Smart Factory

FRA 626 Machine Vision in Smart Factory

Suriya Natsupakpong, PhD

Institute of Field Robotics (FIBO)

King Mongkut's University of Technology Thonburi (KMUTT)

Topics

- Methods of Image Acquisition
- Image Signals
- Image Processing
- Machine Vision Application in Quality Control
- Categorization of Machine Vision Solutions
- General Process for Building Machine Vision Solutions

Methods of Image Acquisition

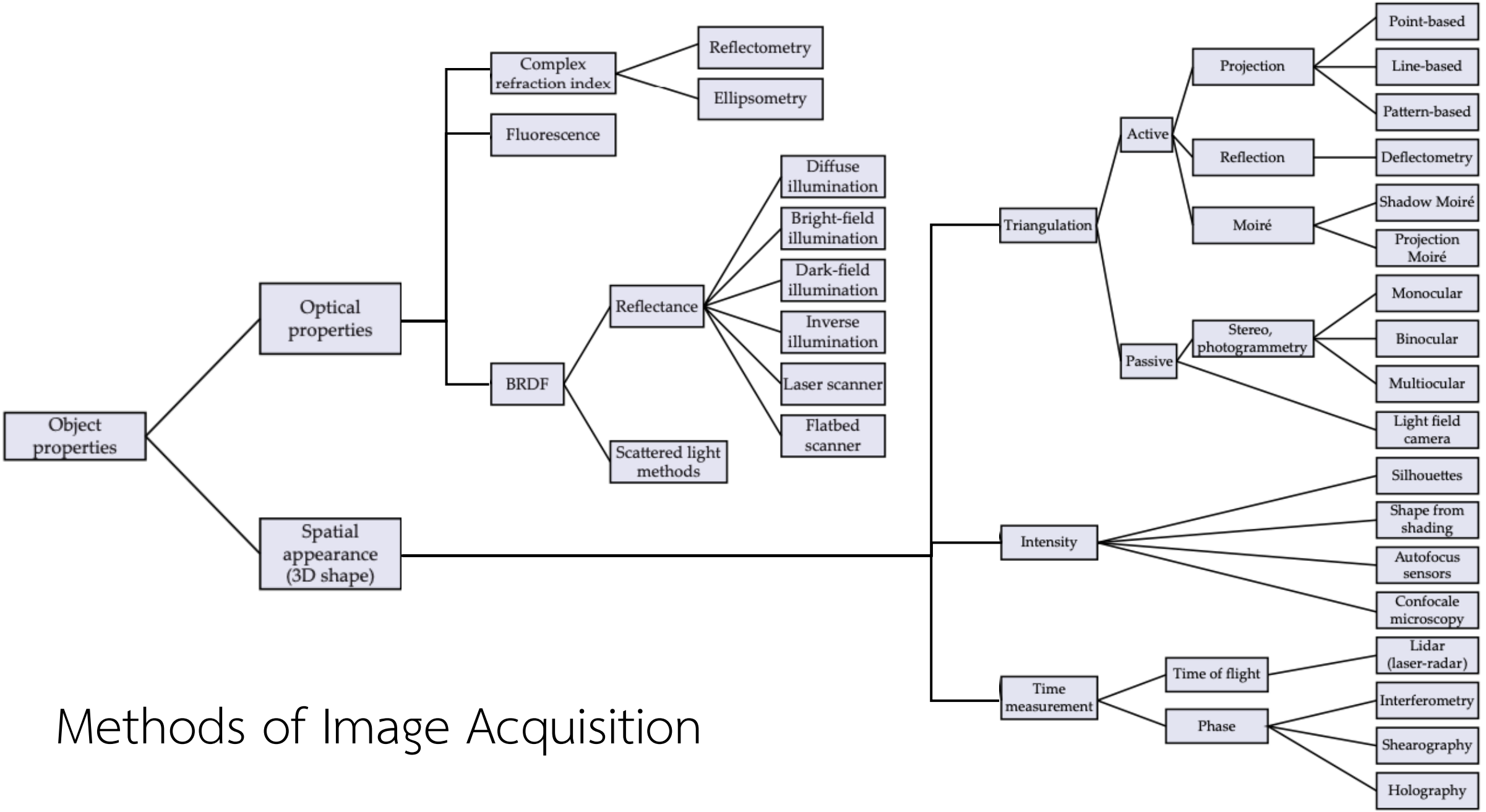

Beyerer, Jürgen & León, F.P. & Frese, C.. (2015). Machine vision: Automated visual inspection: Theory, practice and applications.

The law of refraction

Snell's law of refraction

$$n_1 \sin\theta_1 = n_2 \sin\theta_2$$

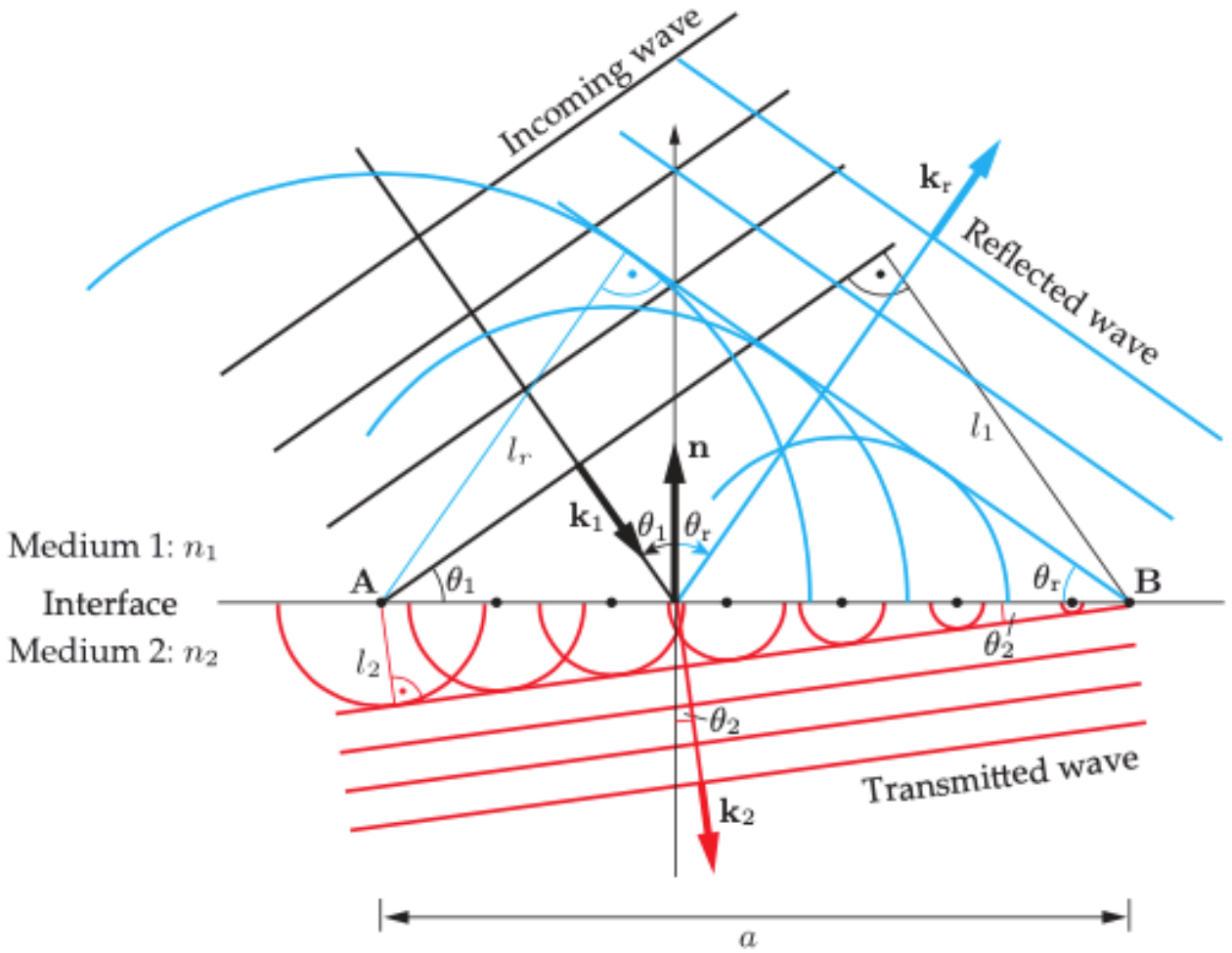

Figure 2.26. Deriving the laws of reflection and refraction by applying Huygens' principle in the plane of incidence.

Beyerer, Jürgen & León, F.P. & Frese, C.. (2015). Machine vision: Automated visual inspection: Theory, practice and applications.

Scattering

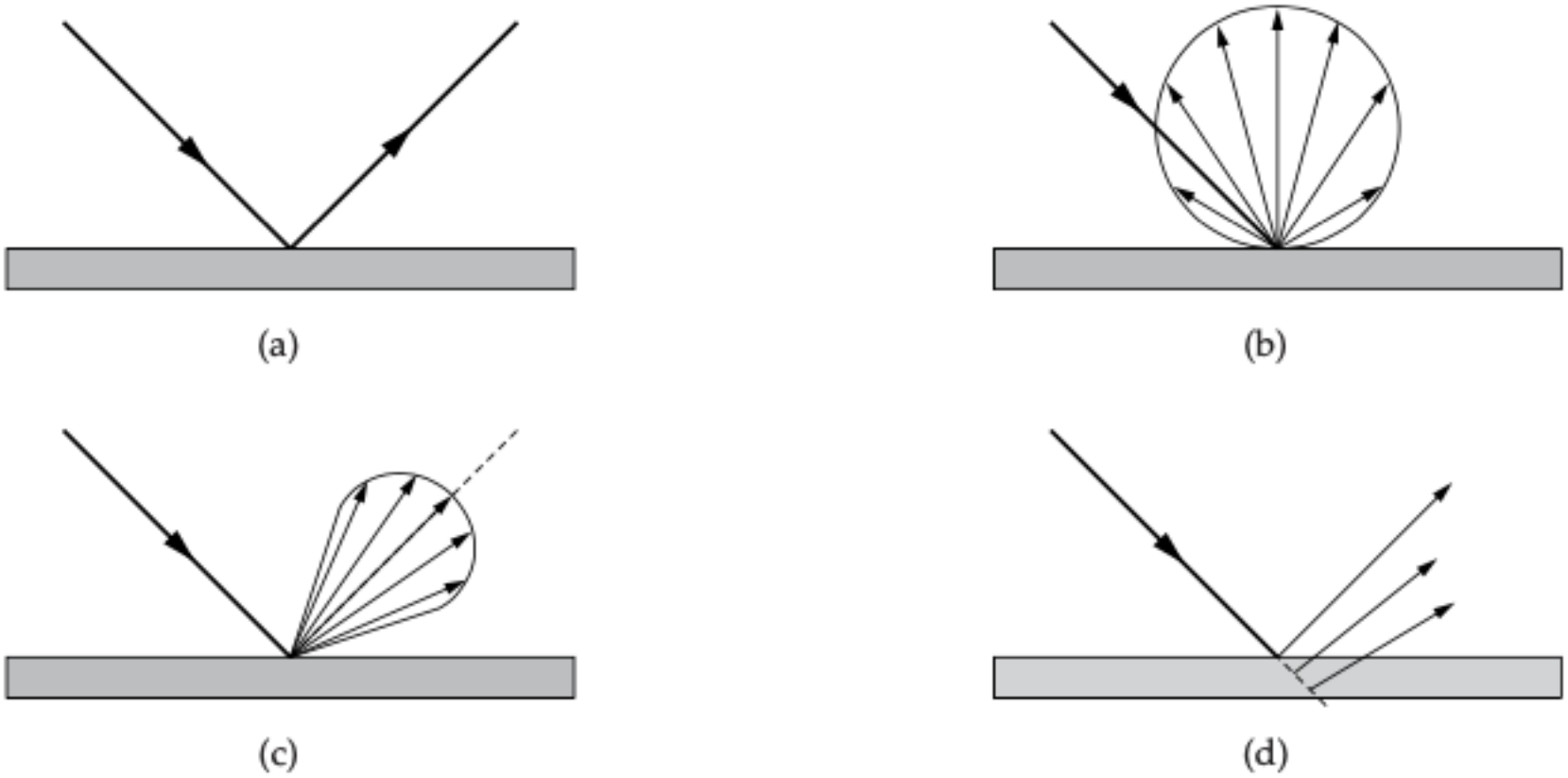

Figure 2.27. Different kinds of scattering caused by surfaces: (a) Perfectly specular reflection; (b) Lambertian reflection; (c) Weakly specular reflection; (d) Volume scattering.

Beyerer, Jürgen & León, F.P. & Frese, C.. (2015). Machine vision: Automated visual inspection: Theory, practice and applications.

Measurement of the complex index of refraction

Reflectometry

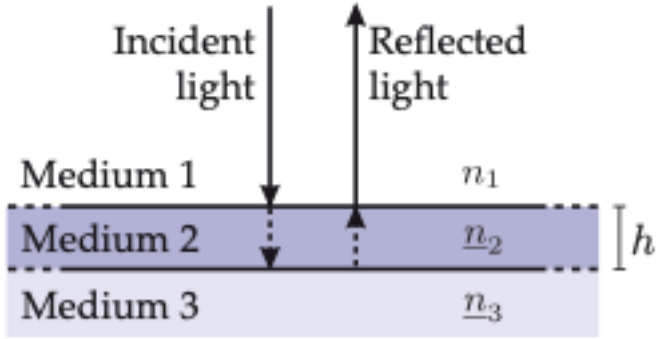

Figure 7.4. Layer model for reflectometry.

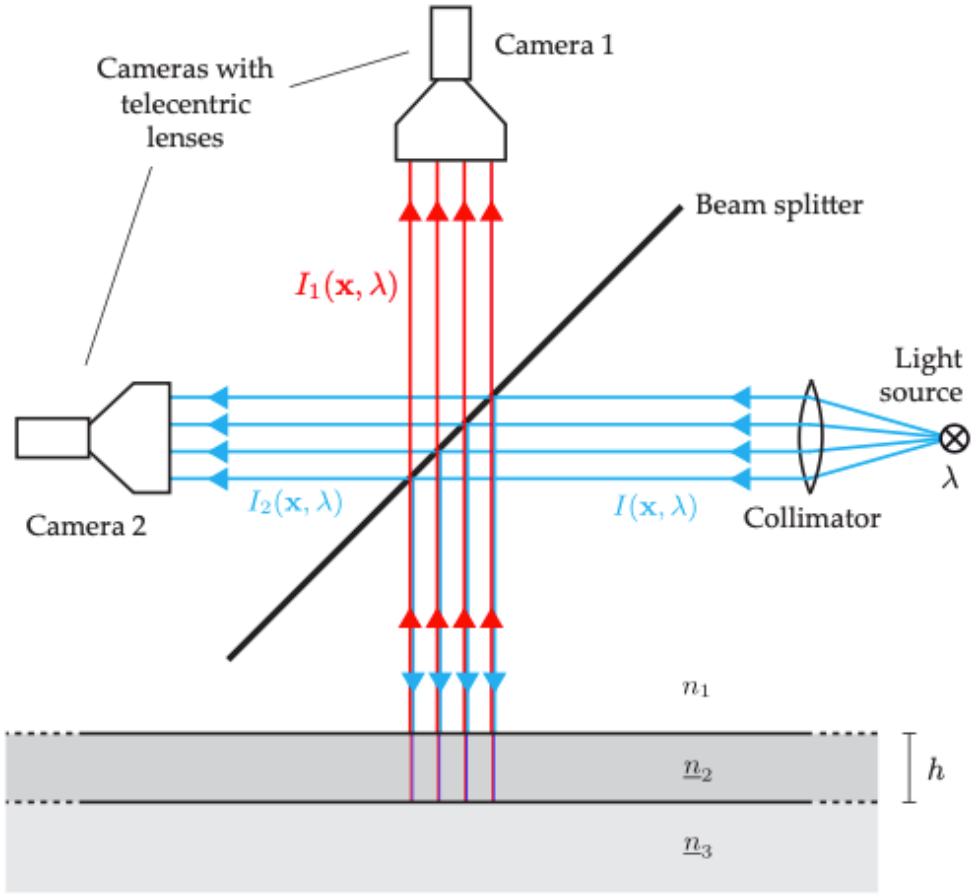

Figure 7.5. Measurement setup for spatially resolved reflectometry.

Beyerer, Jürgen & León, F.P. & Frese, C.. (2015). Machine vision: Automated visual inspection: Theory, practice and applications.

Fluorescence

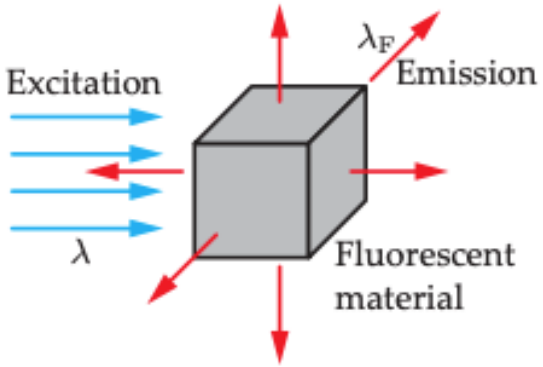

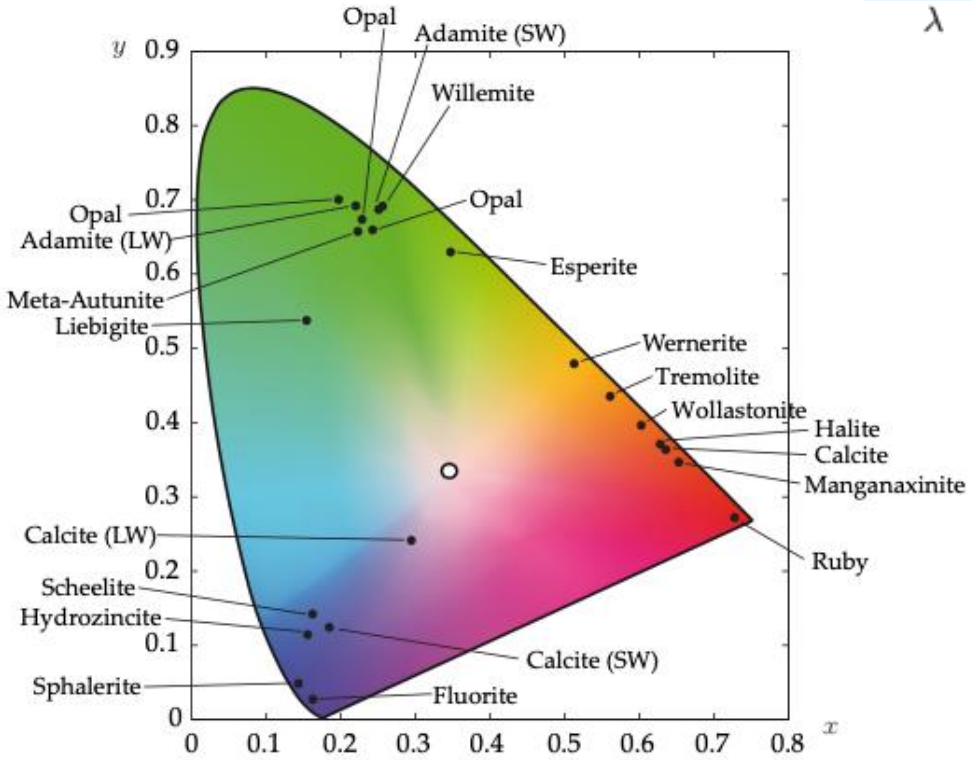

Figure 7.12. Fluorescent colors of minerals [118]. In some cases, different samples of the same mineral from different locations show notably different fluorescent colors. Besides, a material's fluorescence can vary with the spectrum of the exciting light. This figure shows measurements of short-wave UV light (SW, maximum of intensity for $\lambda = 254$ nm) and long-wave UV light (LW, $\lambda = 365$ nm), that corresponds to the spectral lines of a mercury vapor lamp.

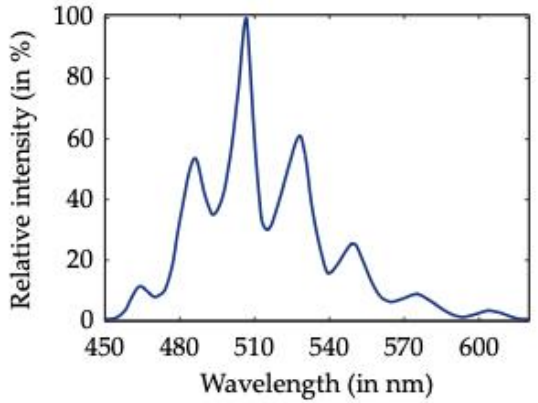

Figure 7.13. Fluorescence spectrum of the mineral liebigite [118].

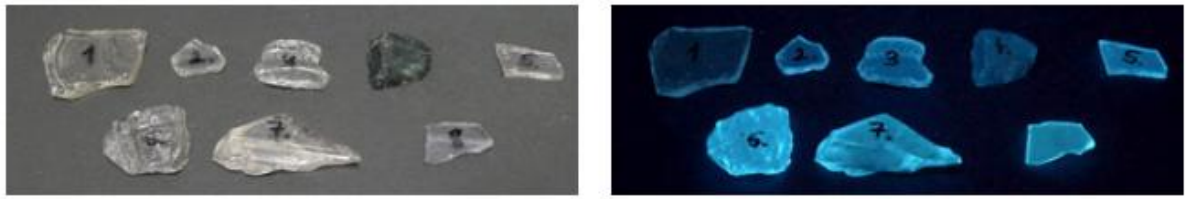

Figure 7.14. Shards of lead glass with varying amounts of lead oxide. (a) Image under white light illumination. (b) Fluorescence under UV illumination, here UV-C illumination of wavelength $\lambda = 254$ nm (mercury line) and an irradiance of 3 $\frac{\text{mW}}{\text{cm}^2}$.

Beyerer, Jürgen & León, F.P. & Frese, C.. (2015). Machine vision: Automated visual inspection: Theory, practice and applications.

Reflectance

Diffuse illumination

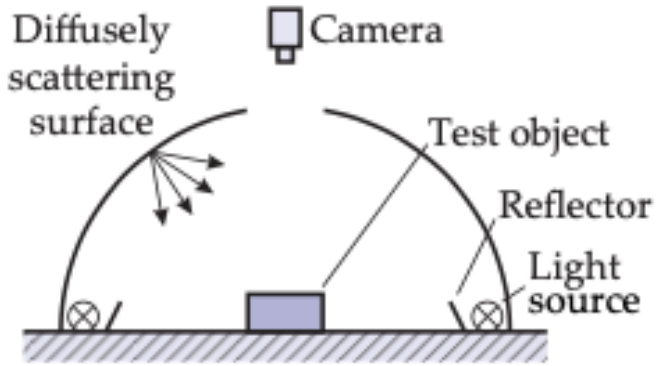

Figure 7.15. Diffuse illumination using a screen in the shape of a hemisphere (adapted from [14]).

Beyerer, Jürgen & León, F.P. & Frese, C.. (2015). Machine vision: Automated visual inspection: Theory, practice and applications.

Reflectance

Bright-field illumination

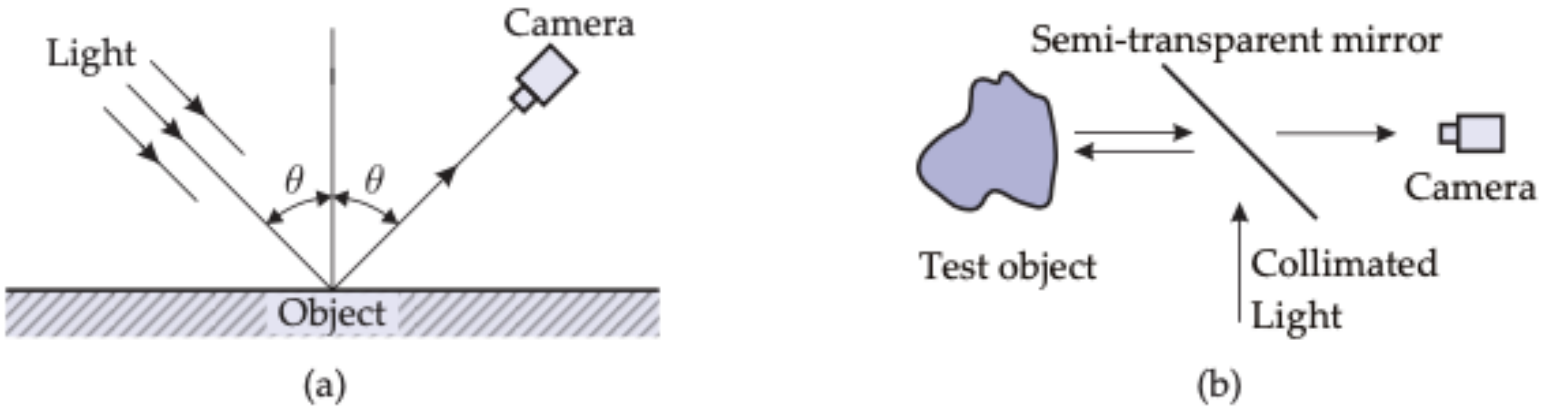

Figure 7.16. Capturing reflectance in bright-field: (a) Principle of bright-field illumination; (b) Coaxial bright-field illumination using a semi-transparent mirror [14].

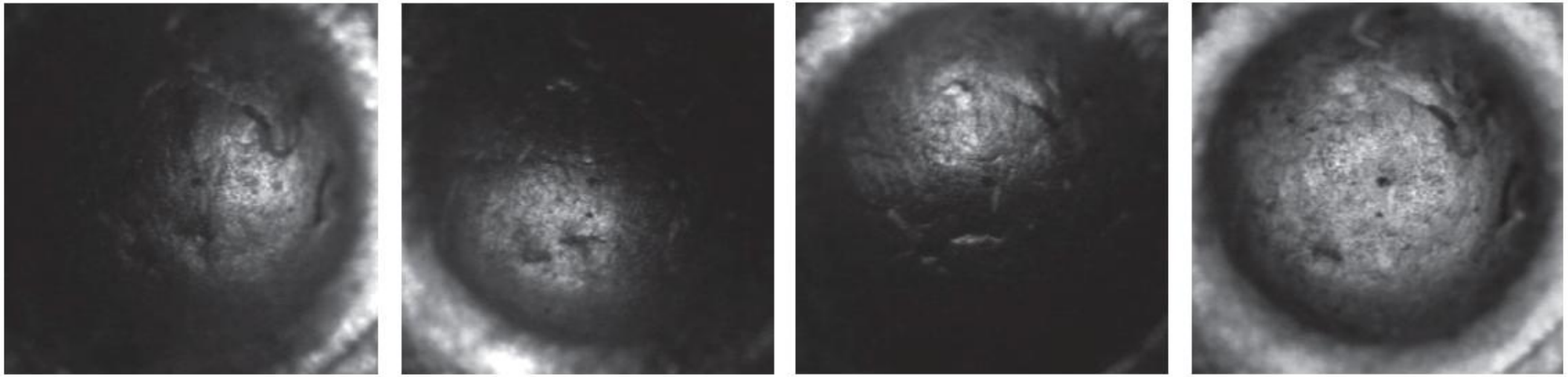

(a) Directional illumination (b) Directional illumination (c) Directional illumination (d) Diffuse illumination

Figure 7.17. Images of the mark left by a firing pin on the back of a bullet casing, taken for automatically identifying firearms: (a)–(c) Directional illumination; (d) Diffuse illumination.

Beyerer, Jürgen & León, F.P. & Frese, C.. (2015). Machine vision: Automated visual inspection: Theory, practice and applications.

Reflectance

Dark-field illumination

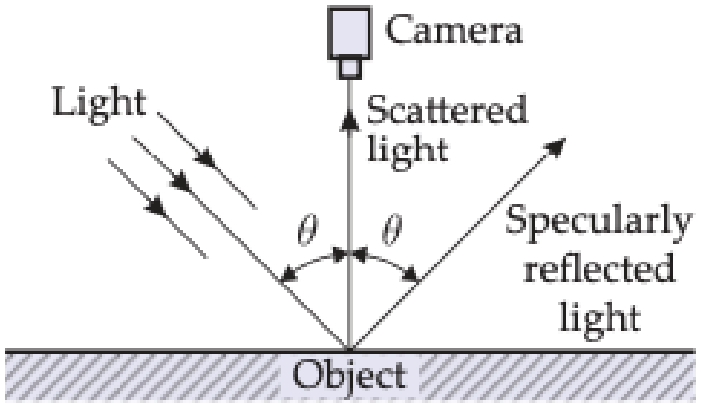

Figure 7.18. Dark-field illumination.

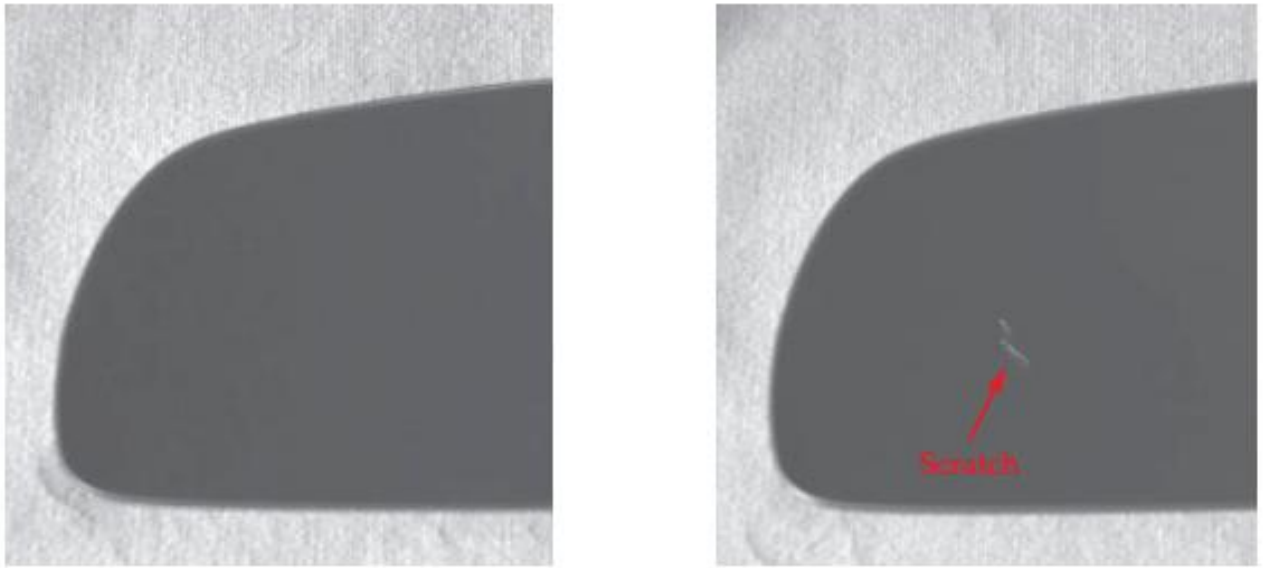

Figure 7.19. Dark field illuminated images of wing mirrors for the detection of scratches: (a) Reference object; (b) Test object with scratches.

Beyerer, Jürgen & León, F.P. & Frese, C.. (2015). Machine vision: Automated visual inspection: Theory, practice and applications.

Bright or Dark Field Lighting in Applications

Bright Field Lighting

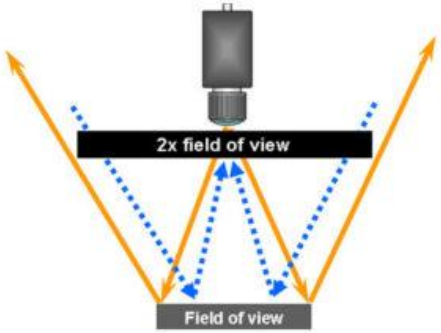

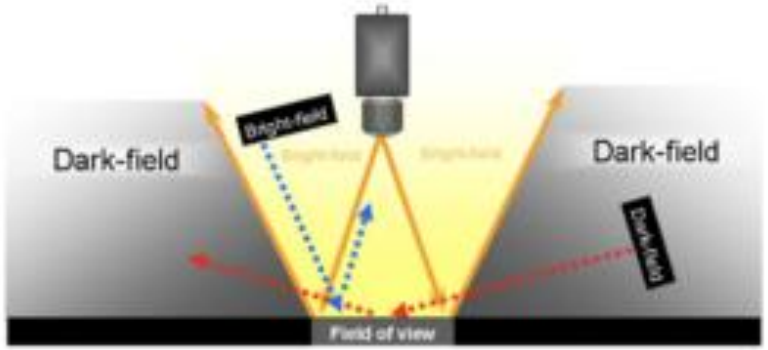

Dark Field Lighting

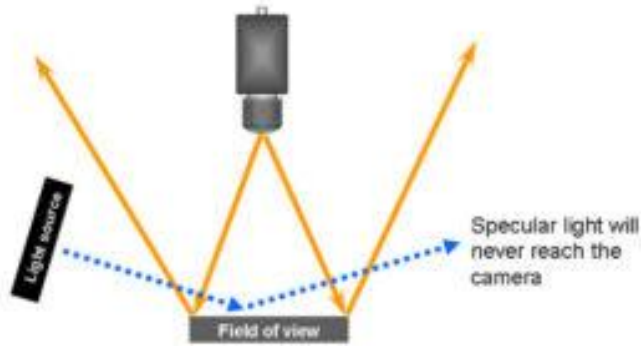

dark field is advantageous when imaging things such as reflective surfaces and edge inspections. a low angle of light (usually from ring lights) of around 10-15 degrees is ideal.

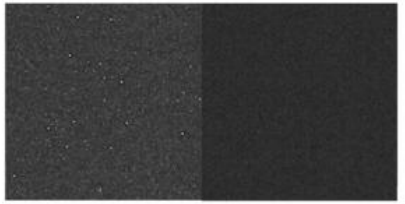

Dark Signal Non-Uniformity (DSNU) calibration.

https://www.adimec.com/exploring-bright-field-versus-dark-field-lighting-for-your-inspection-application/

Reflectance

Laser scanners

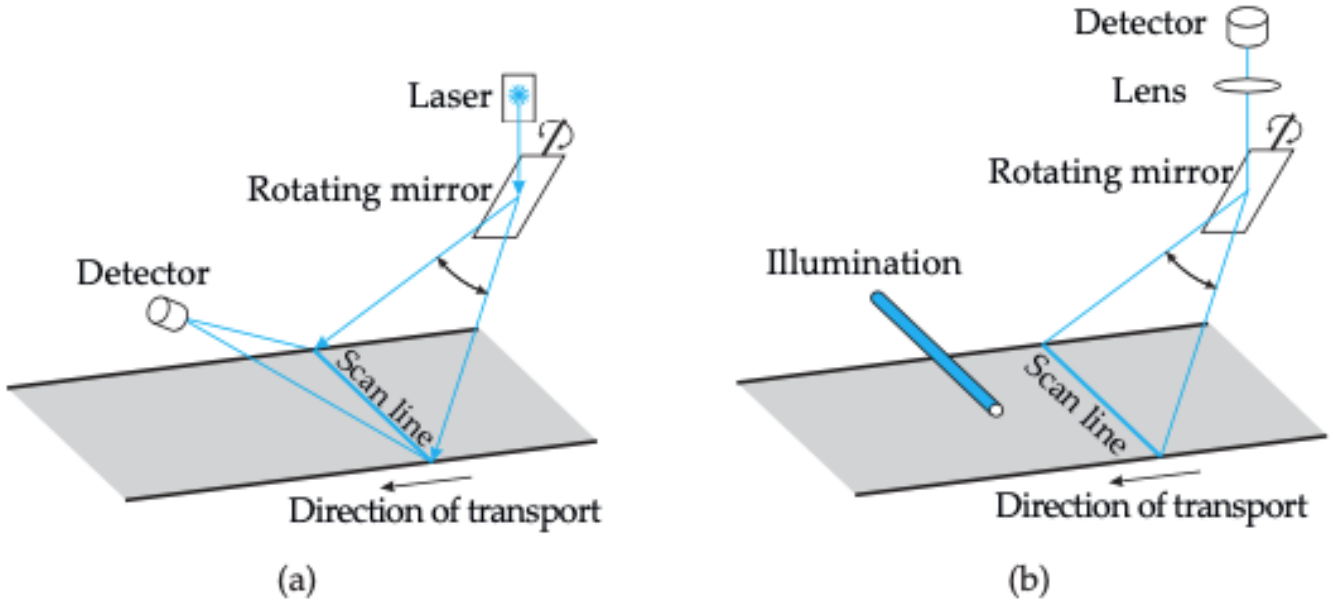

Figure 7.21. Visual inspection of continuous products with a scanning image acquisition: (a) Flying-spot scanner; (b) Flying-image scanner (adapted from [49]).

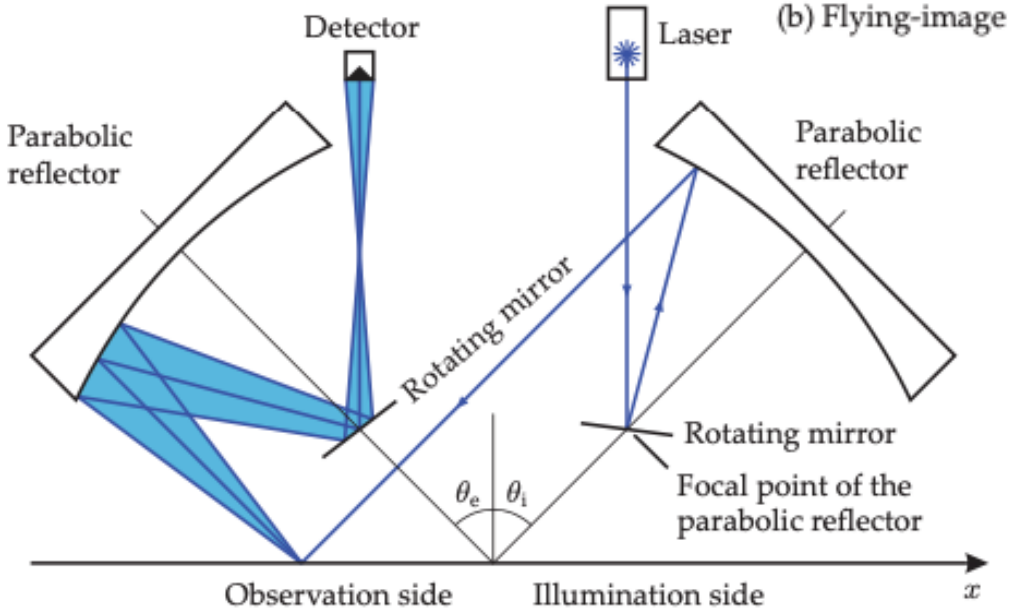

Figure 7.22. Setup of a telecentric laser scanner with two parabolic reflectors (adapted from [49]).

Beyerer, Jürgen & León, F.P. & Frese, C.. (2015). Machine vision: Automated visual inspection: Theory, practice and applications.

Reflectance

Flatbed scanners

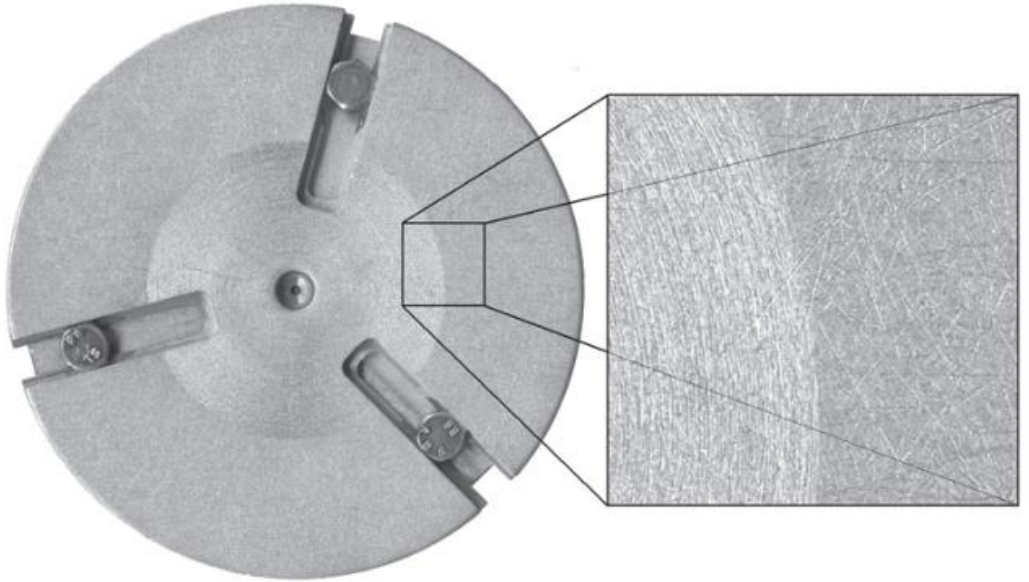

Figure 7.23. Image of a metal flange with a diameter of about 15 cm, acquired with a flatbed scanner. The magnification on the right shows that the image has a high resolution and fine details, e.g., scratches are clearly visible.

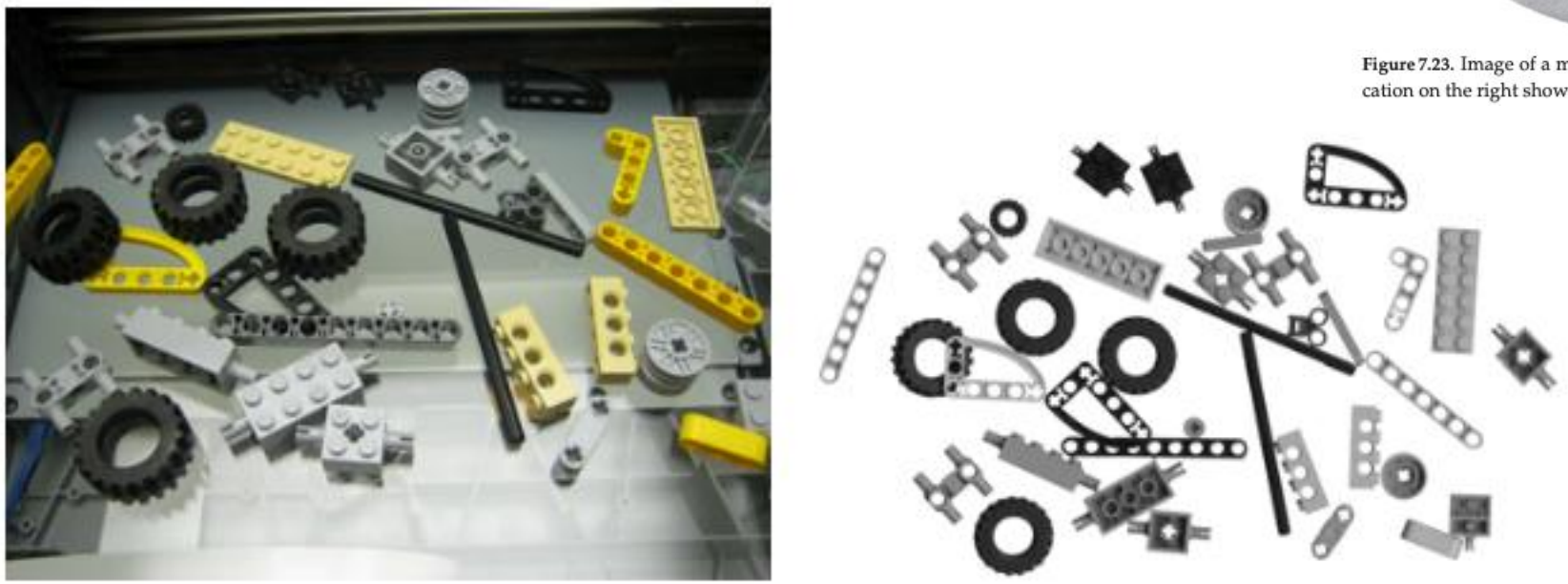

(a) (b)

Figure 7.24. Checking the completeness of a toy construction kit: (a) Camera image; the analysis is complicated by perspective distortions and reflections; (b) This image of the same scene taken by a flatbed scanner is homogeneously illuminated and free of distortions.

Beyerer, Jürgen & León, F.P. & Frese, C.. (2015). Machine vision: Automated visual inspection: Theory, practice and applications.

Light scattering methods

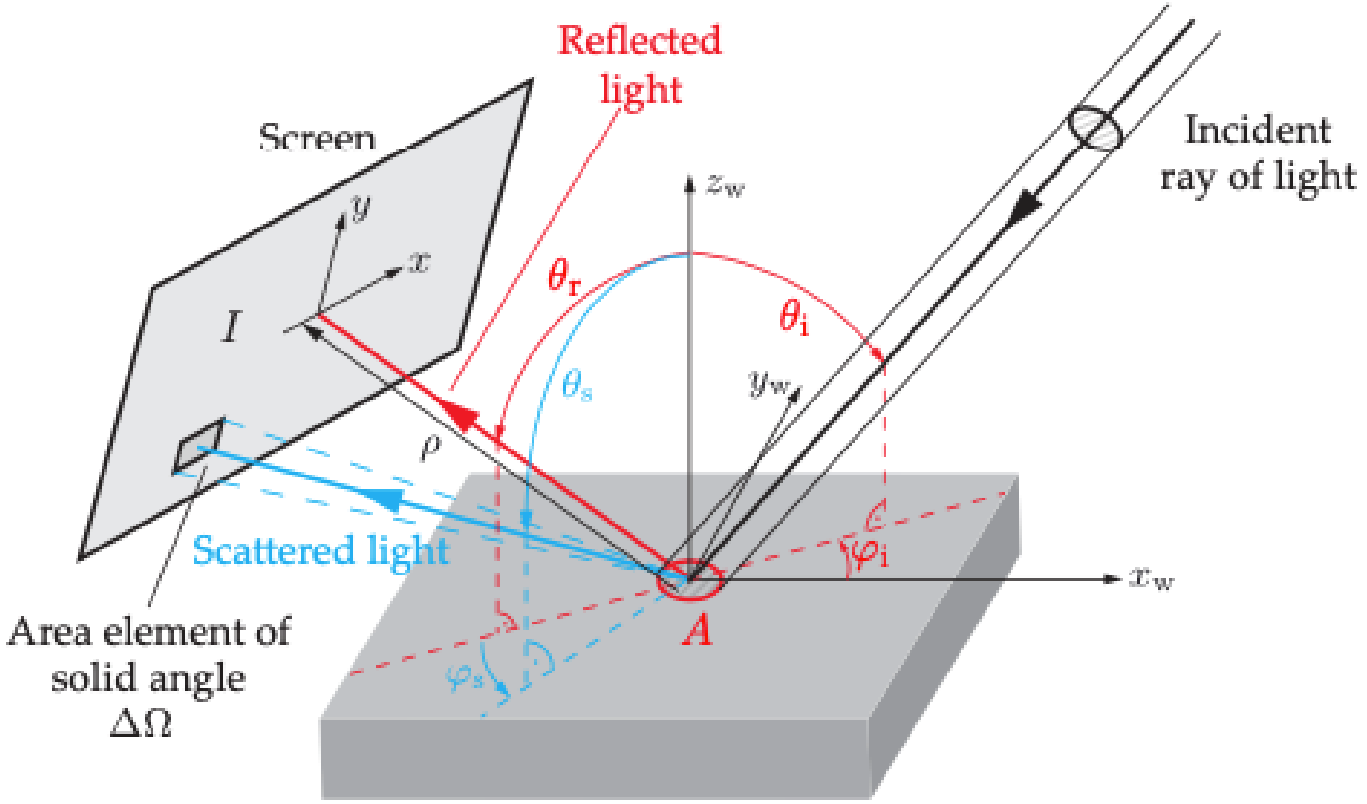

Figure 7.29. Setup for measuring scattered light.

Beyerer, Jürgen & León, F.P. & Frese, C.. (2015). Machine vision: Automated visual inspection: Theory, practice and applications.

Light scattering methods

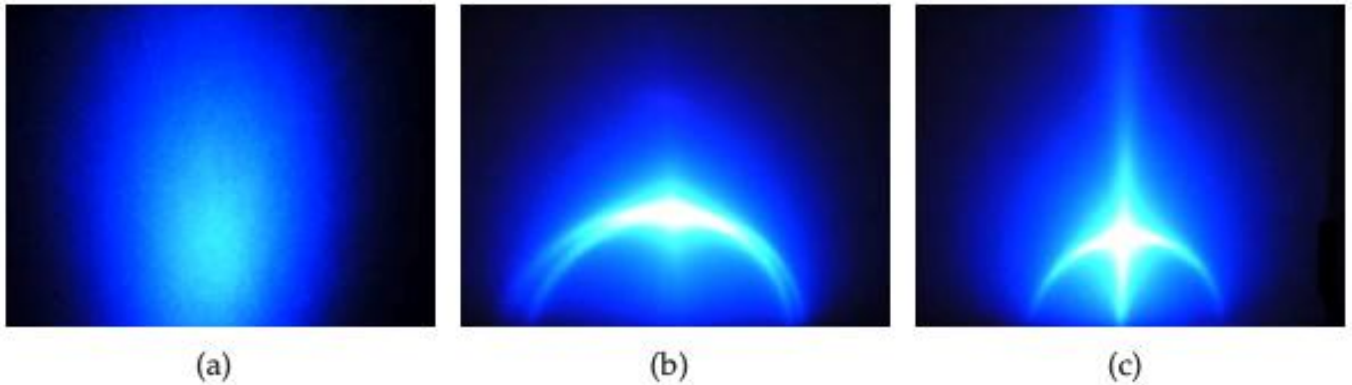

Figure 7.31. Light scattering images of different surfaces: (a) Sandblasted steel; (b) Smoothed steel surface with a set of grooves; (c) Ground steel with two series of rills intersecting under an angle of 90°; (d) Aluminum foil, rough side (e) Aluminum foil, smooth side.

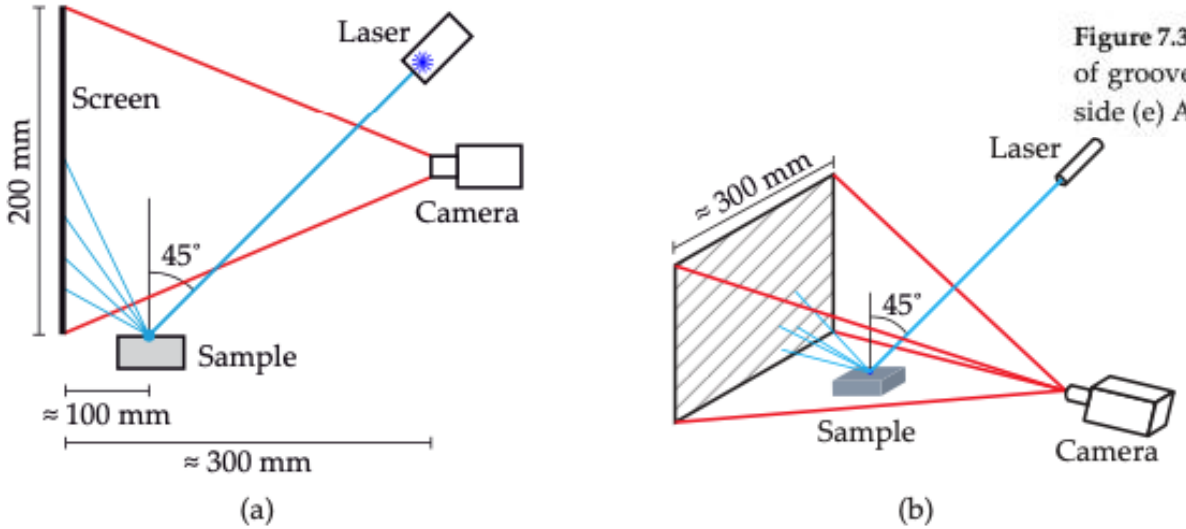

Figure 7.30. Example of a setup for capturing scattered light images.

Beyerer, Jürgen & León, F.P. & Frese, C.. (2015). Machine vision: Automated visual inspection: Theory, practice and applications.

3D shape capturing

Light-section methods (line scanning)

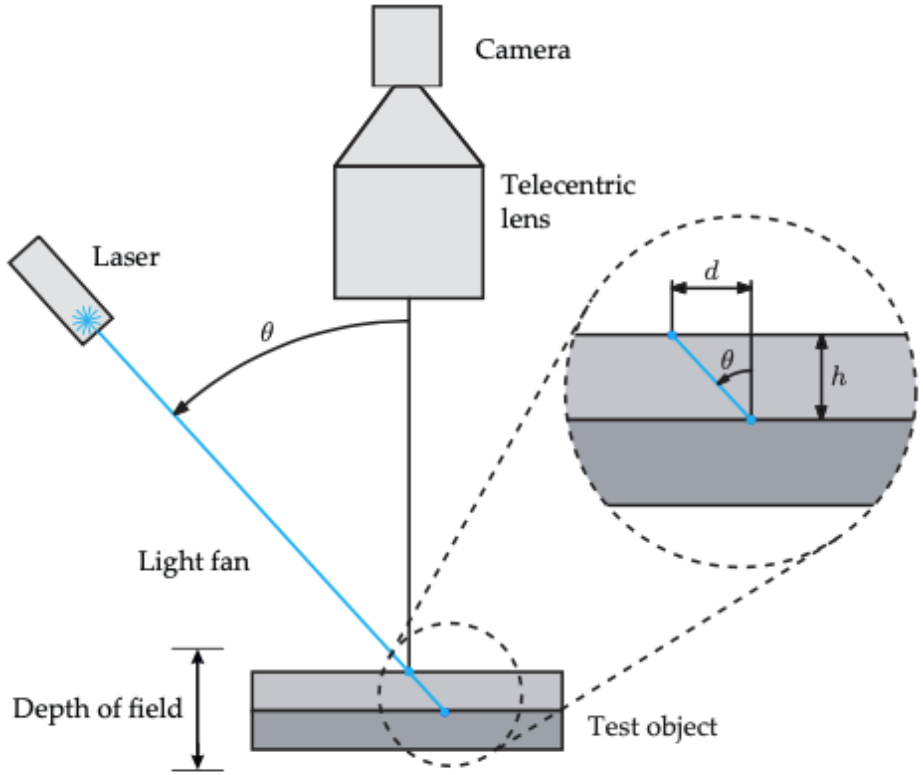

Figure 7.38. Calculation of the height difference for the light-section method.

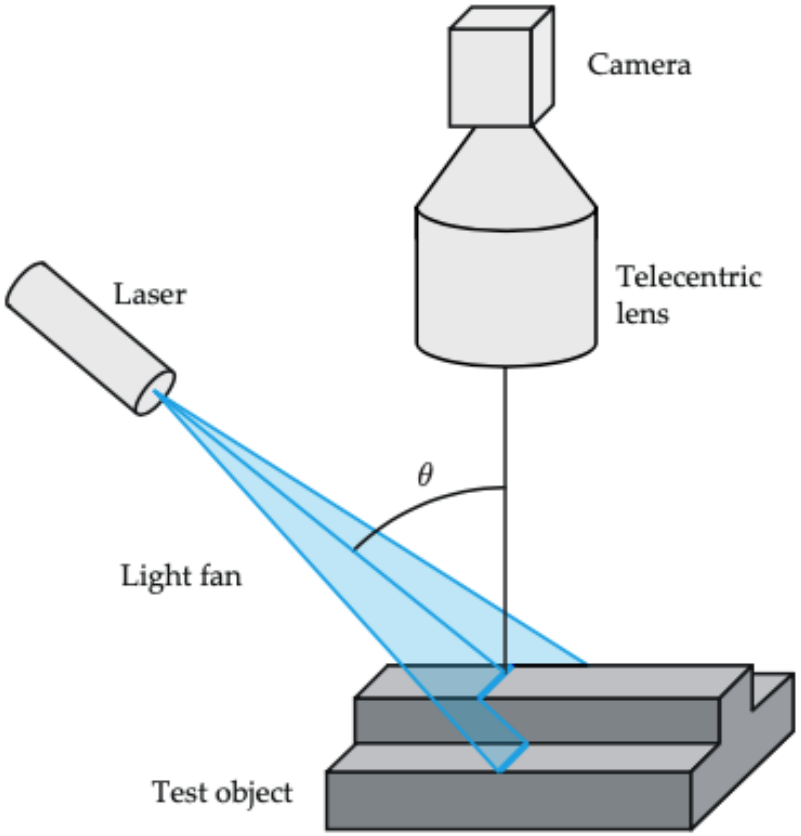

Figure 7.37. Light-section sensor with telecentric observation, used for depth measurement based on the principle of triangulation.

Beyerer, Jürgen & León, F.P. & Frese, C.. (2015). Machine vision: Automated visual inspection: Theory, practice and applications.

3D shape capturing

Structured illumination

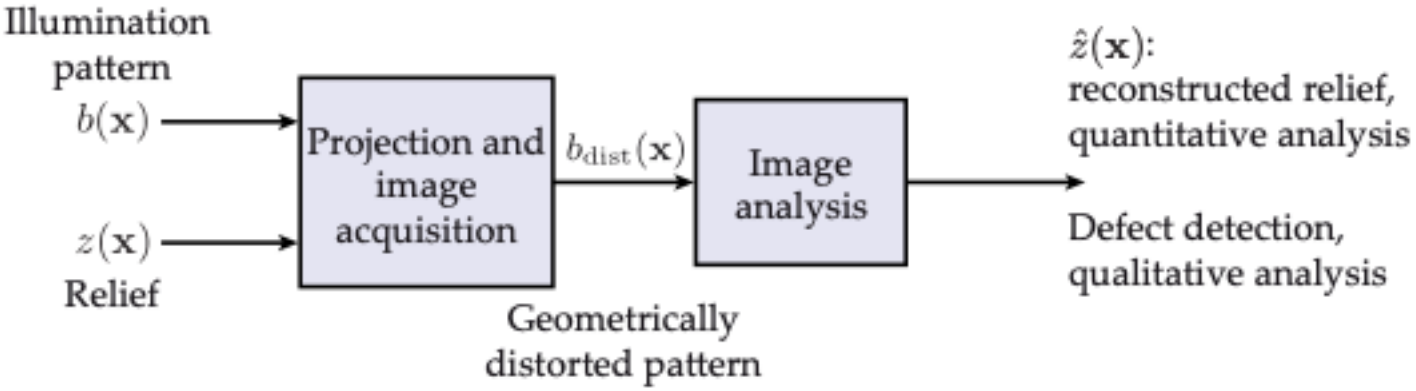

Figure 7.41. Signal model of pattern projection.

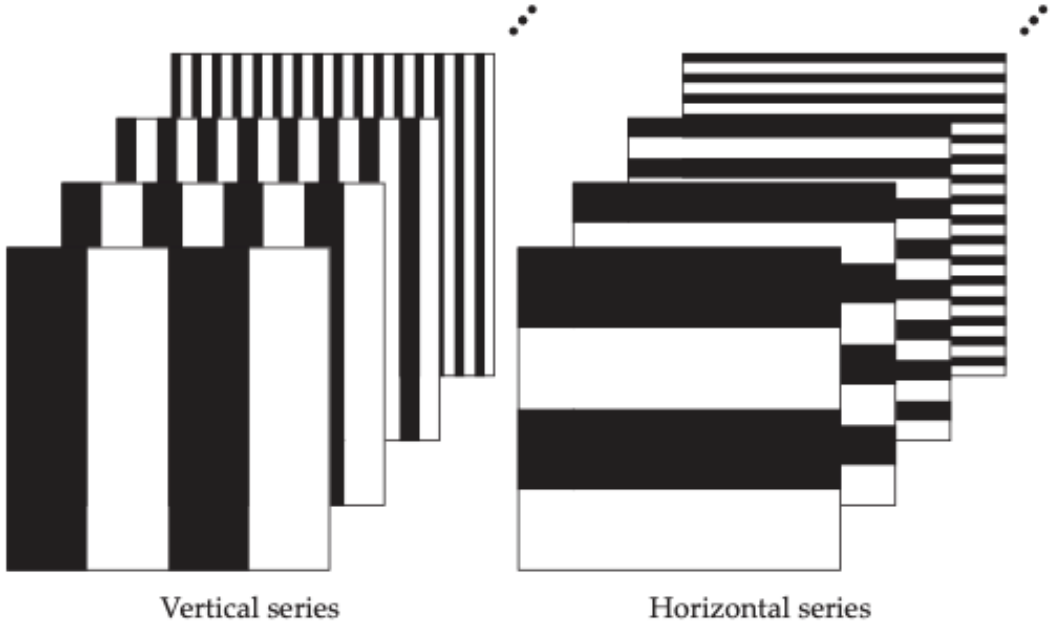

Figure 7.42. Image series used for binary coding the pixel position in the projected pattern.

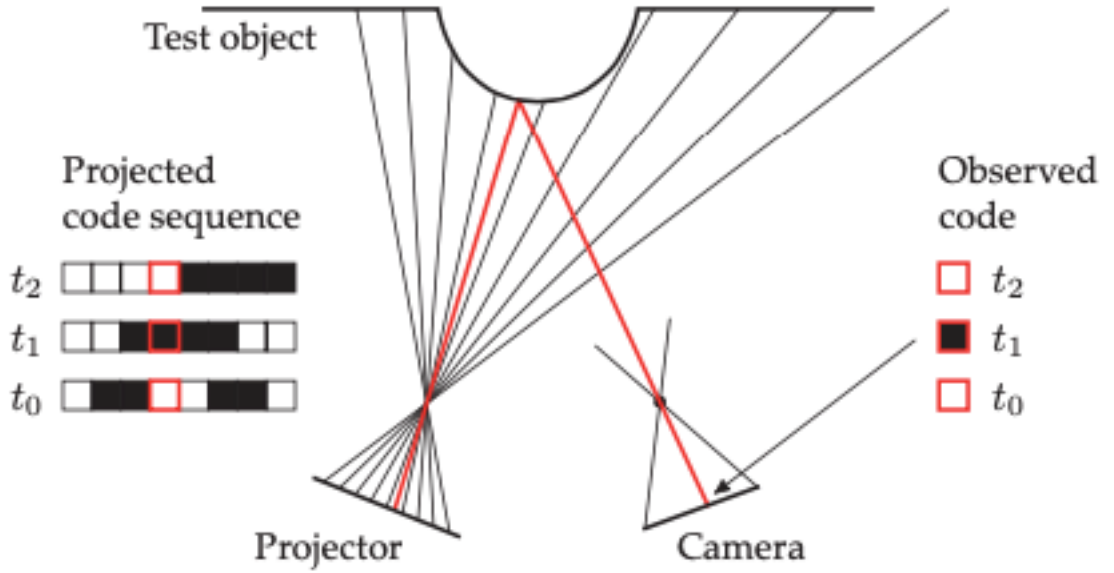

Figure 7.43. Decoding a pixel coordinate from successive Gray code images.

Beyerer, Jürgen & León, F.P. & Frese, C.. (2015). Machine vision: Automated visual inspection: Theory, practice and applications.

3D shape capturing

Structured illumination

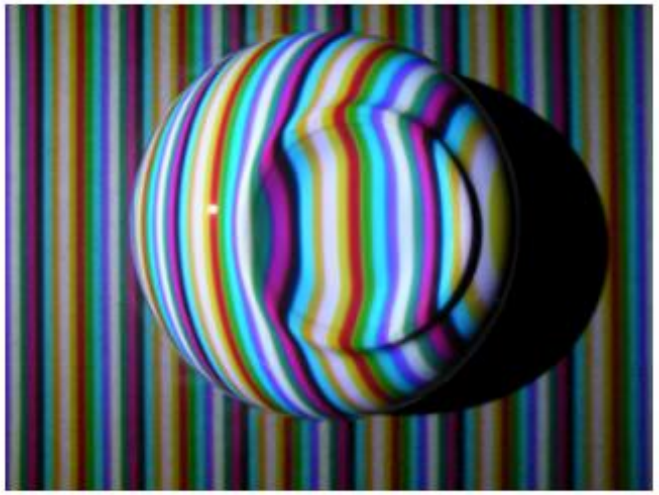

Figure 7.44. Projection of a periodic pattern of colored stripes on a sample scene consisting of a cup placed upside down on a sheet of paper. Some colors like white, yellow and blue occur multiple times in one period, but can be unambiguously identified because of the neighboring stripes.

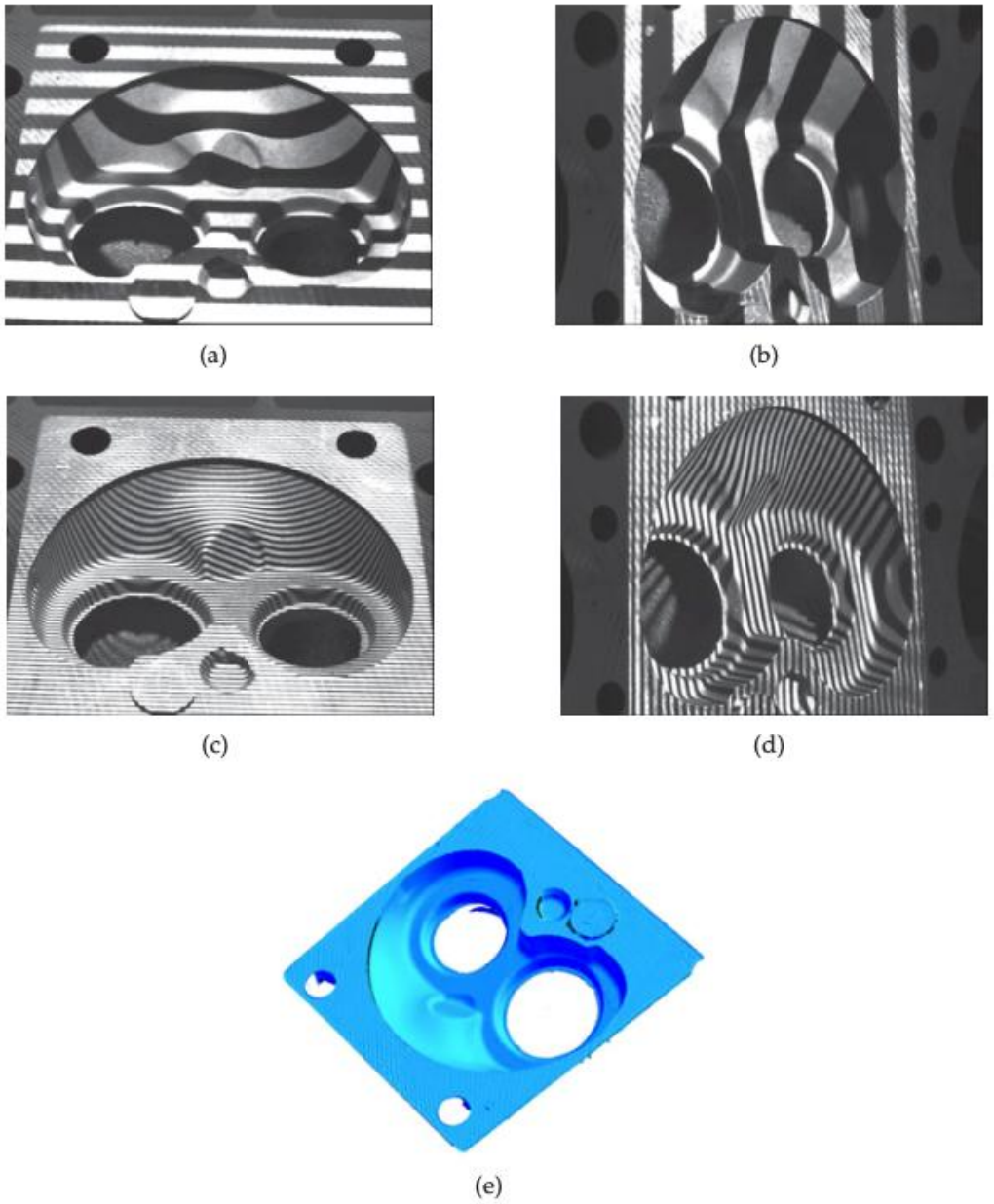

Figure 7.45. Inspection of the combustion chamber of a cylinder head: (a)–(d) Single images of the projected sequence of stripe patterns; (e) 3D reconstruction (source: inspectomation GmbH).

Beyerer, Jürgen & León, F.P. & Frese, C.. (2015). Machine vision: Automated visual inspection: Theory, practice and applications.

3D shape capturing

Deflectometry

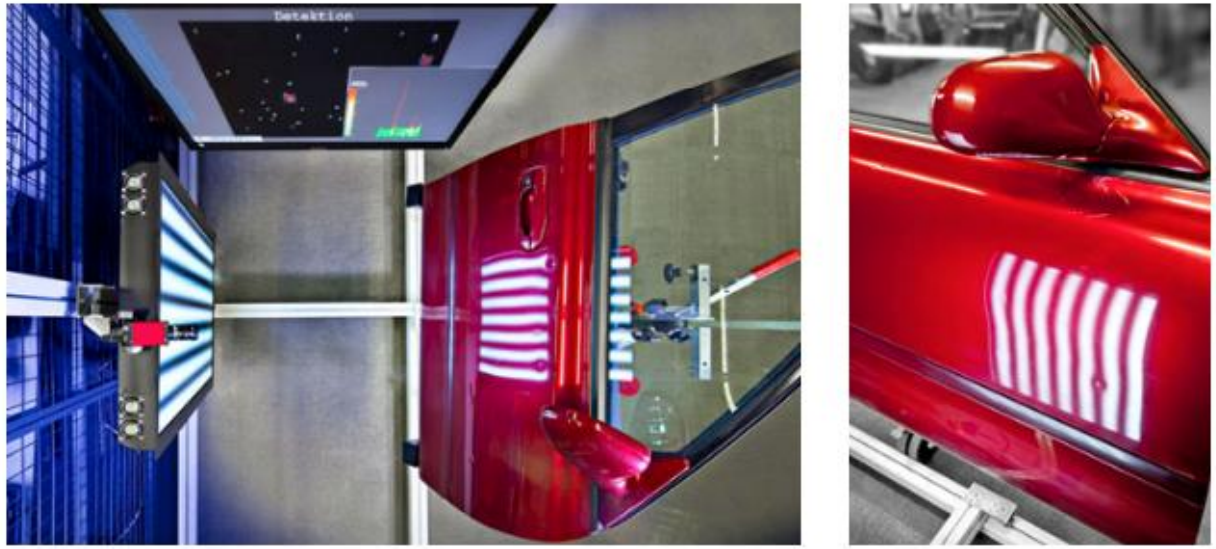

(a) (b)

Figure 7.47. Deflectometric setup for the inspection of a coated car door: (a) Setup of pattern generator, test object and camera; (b) When observing the reflected stripe pattern, a defect is clearly visible.

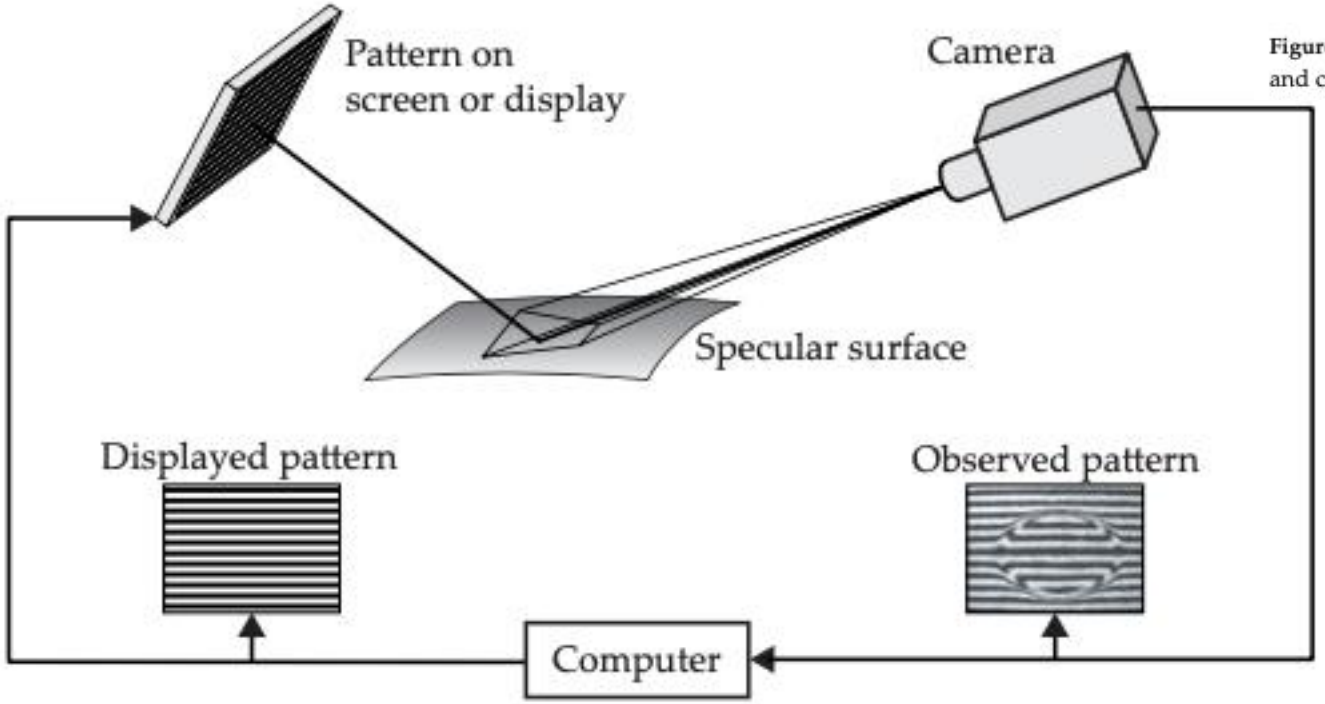

Figure 7.46. Setup of pattern generator and camera for deflectometry.

(a) Horizontal stripe pattern (b) Vertical stripe pattern

Figure 7.50. Image of a transparent object acquired using deflectometry and transmitted light.

Beyerer, Jürgen & León, F.P. & Frese, C.. (2015). Machine vision: Automated visual inspection: Theory, practice and applications.

3D shape capturing

The moiré method

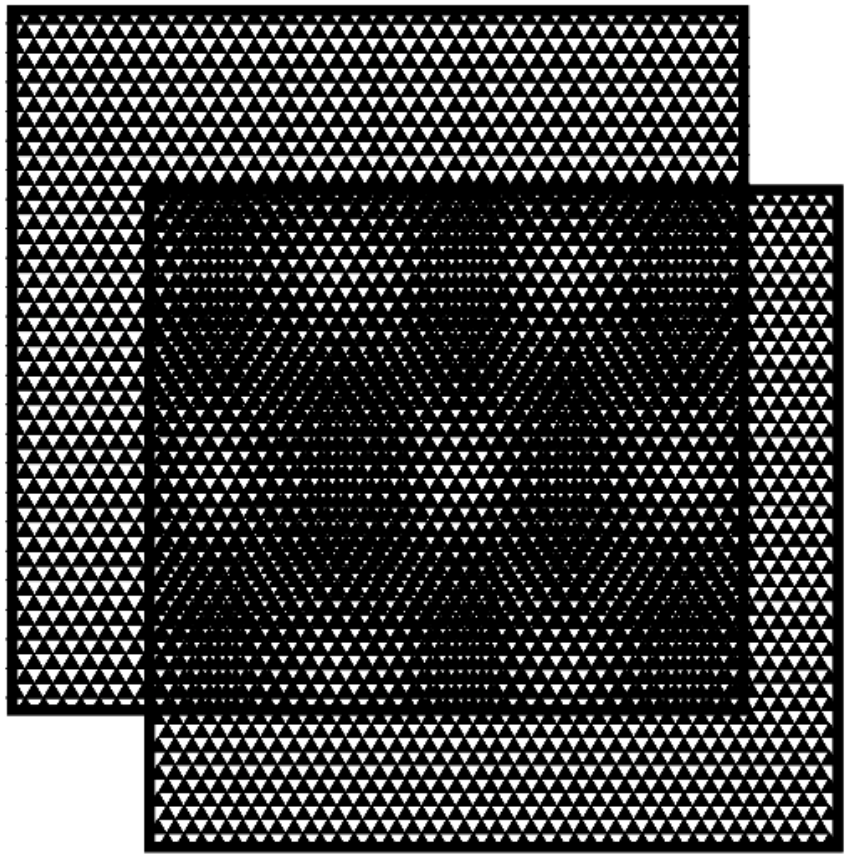

Figure 7.58. Moiré effect caused by the superposition of two triangle patterns with slightly different scales.

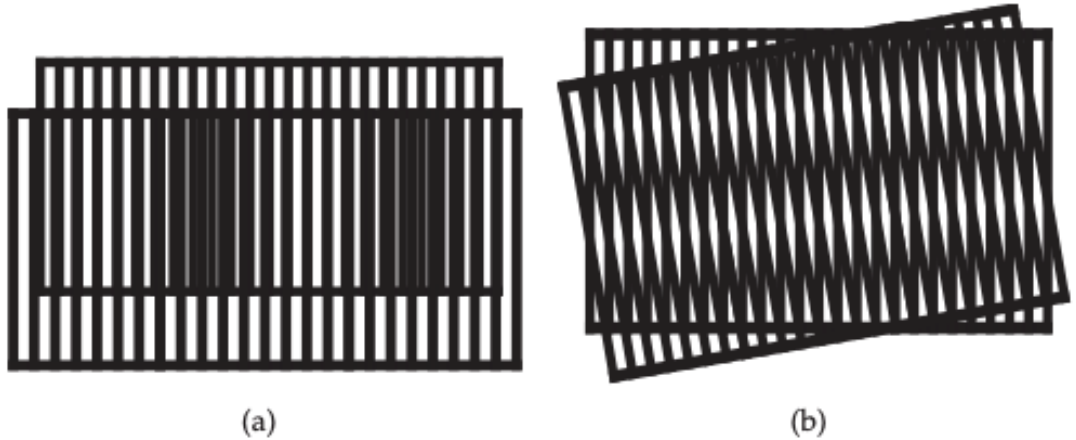

Figure 7.57. Moiré effect caused by the superposition of two stripe structures: (a) Different stripe distances; (b) Rotated stripe pattern.

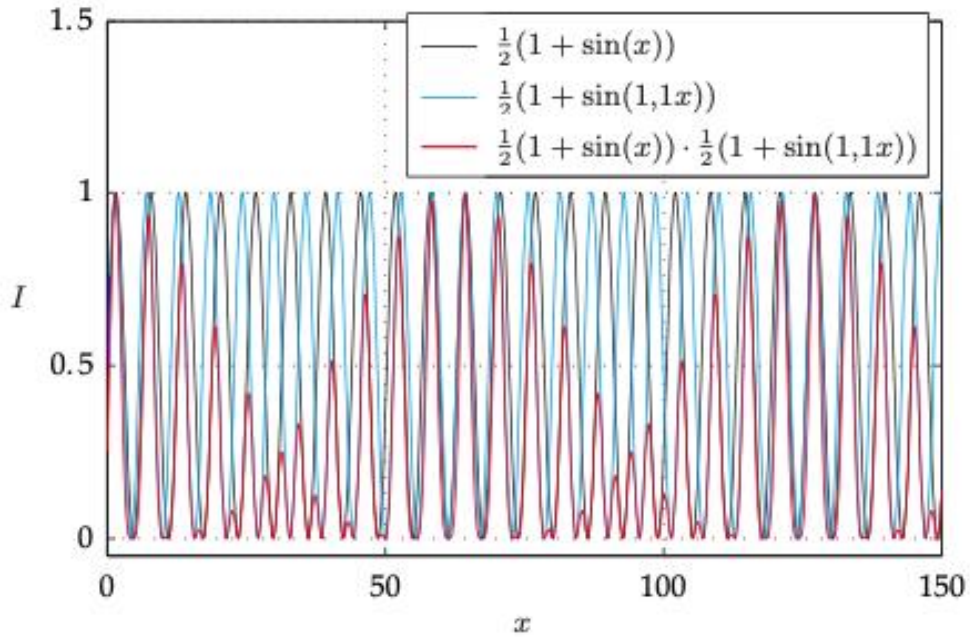

Figure 7.59. Moiré effect caused by the multiplicative superposition of two sine waves. The base frequency of the moiré oscillation corresponds to the difference between the two original frequencies, in accordance with (7.77) and (7.78).

Beyerer, Jürgen & León, F.P. & Frese, C.. (2015). Machine vision: Automated visual inspection: Theory, practice and applications.

3D shape capturing

Light-field cameras

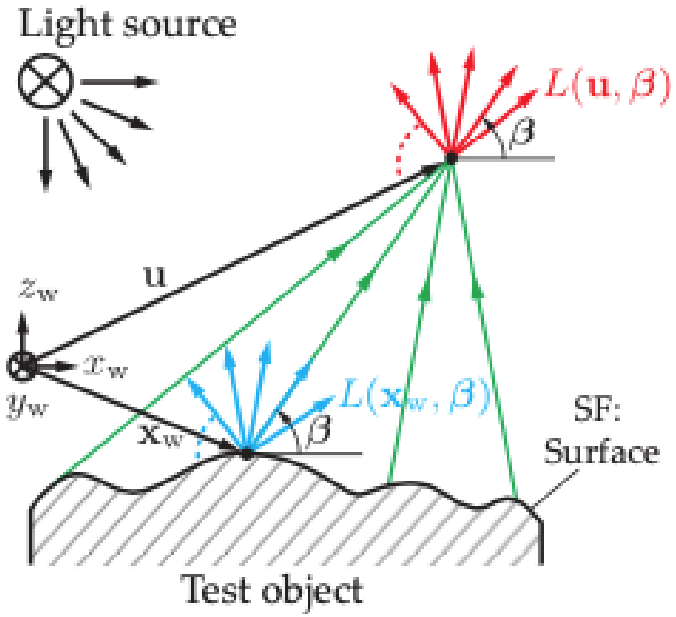

Figure 7.69. Light field of a test object.

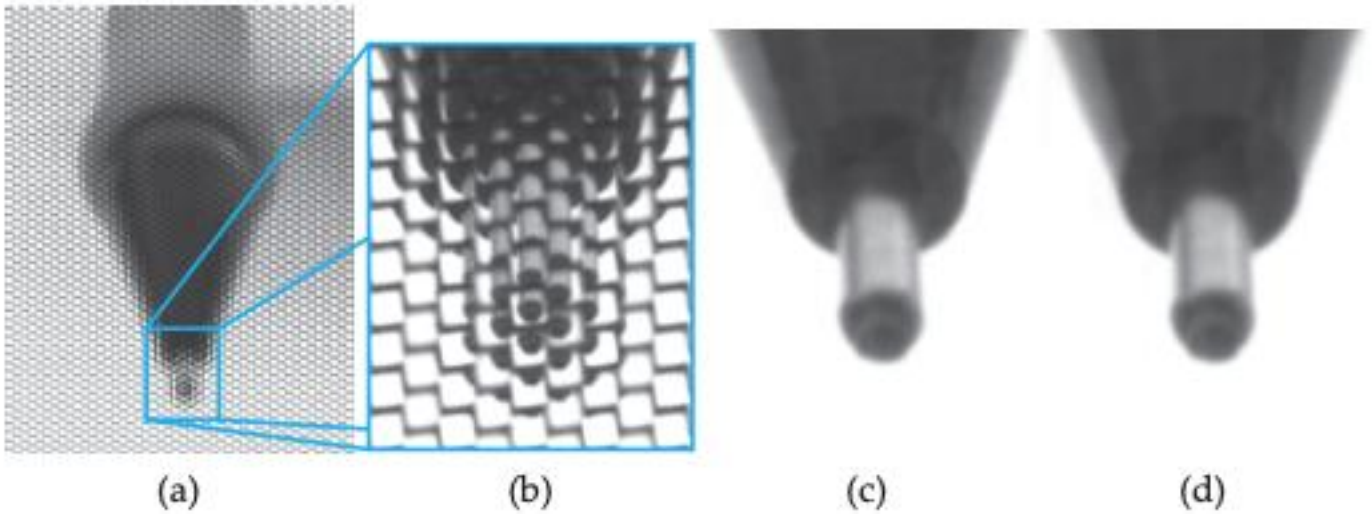

Figure 7.71. Image of the top of a drop action pencil recorded with a light-field camera: (a) Raw data of the image sensor; (b) Section of the pencil's top, the regions of the single microlenses are clearly visible; (c), (d) Images synthesized from the raw data with horizontally displaced perspectives.

Beyerer, Jürgen & León, F.P. & Frese, C.. (2015). Machine vision: Automated visual inspection: Theory, practice and applications.

3D shape capturing

Silhouette capturing

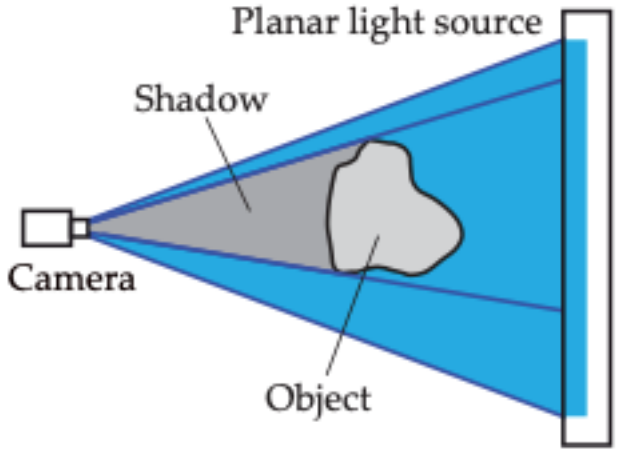

Figure 7.72. Silhouette capturing with bright field illumination.

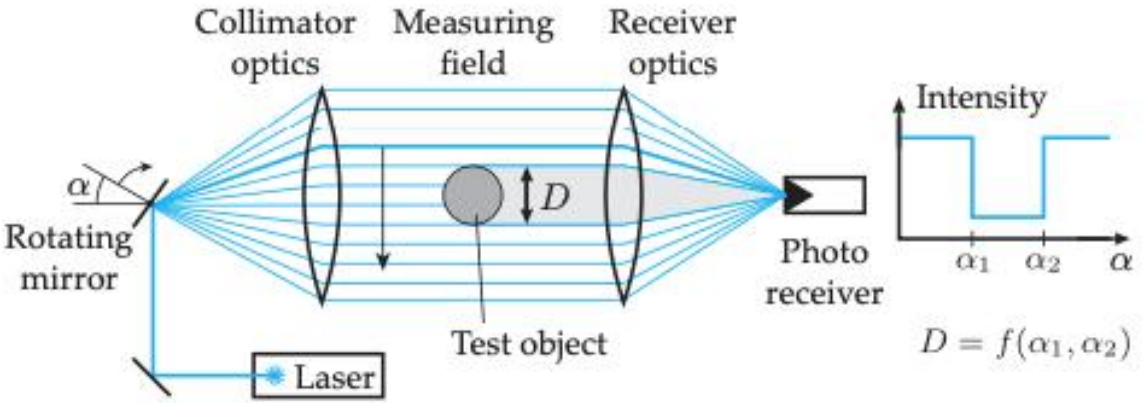

Figure 7.74. Using a telecentric laser scanner for silhouette capturing in accordance with the principle of shadow casting [163]).

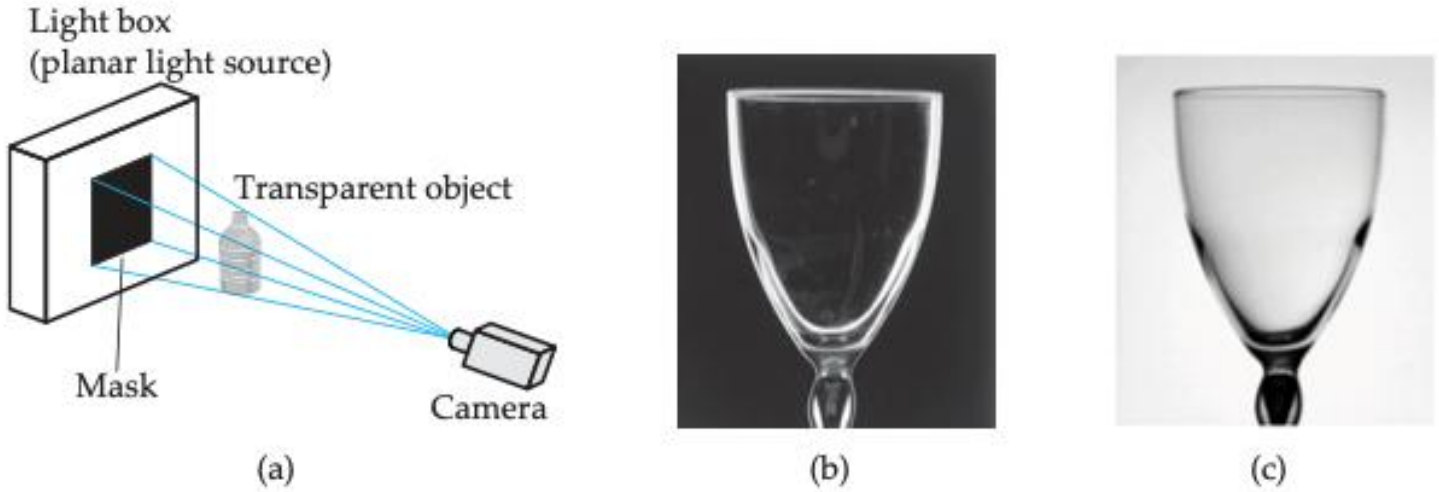

Figure 7.75. Dark-field illumination used for capturing the silhouette of transparent objects: (a) Principle [14]; (b) Dark-field image; (c) Bright-field image of the same object.

Beyerer, Jürgen & León, F.P. & Frese, C.. (2015). Machine vision: Automated visual inspection: Theory, practice and applications.

3D shape capturing

Shape from shading

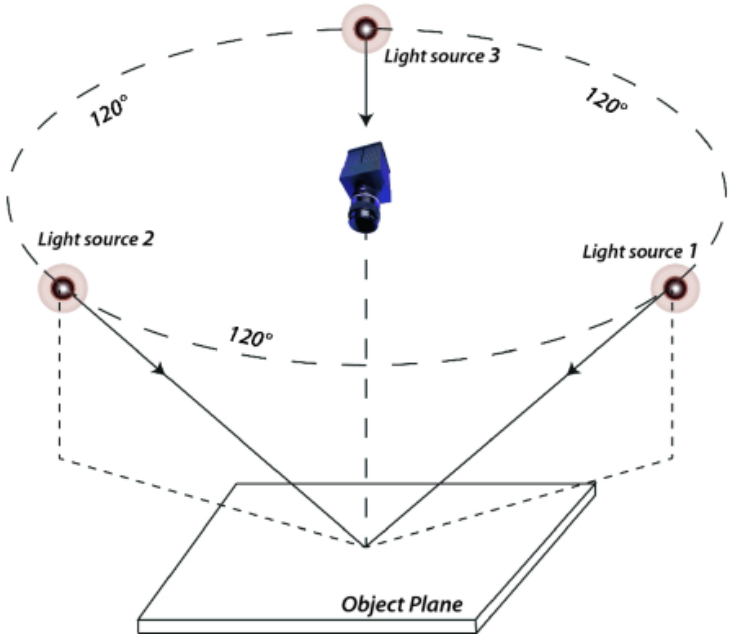

https://link.springer.com/chapter/10.1007/978-3-030-42378-0_5

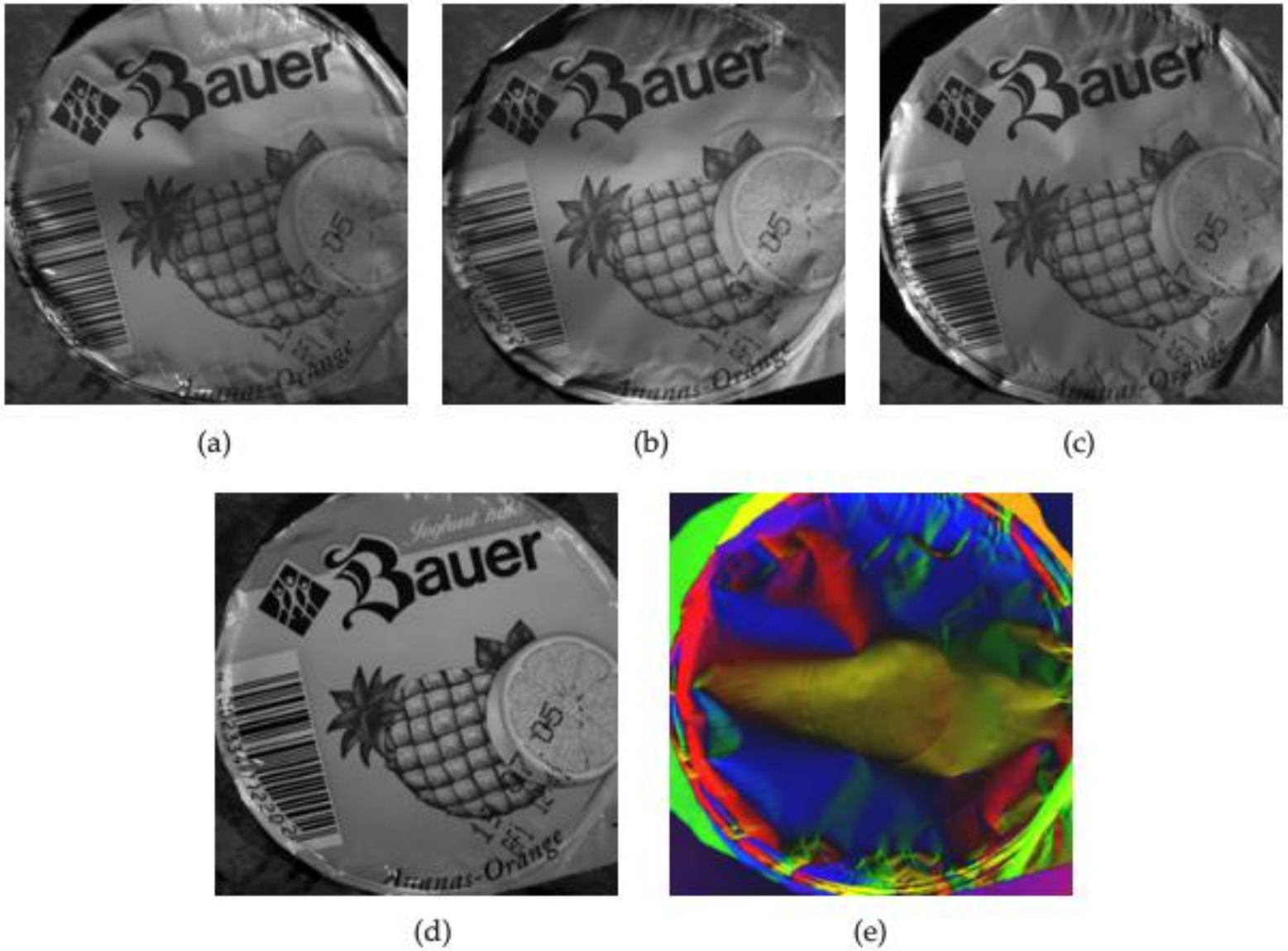

Figure 7.81. Example images of shape from shading: (a)–(c) Images of a packaging foil with different illumination directions; (d) Calculated reflectance $R(\mathbf{x})$; (e) Normal field $\mathbf{n}(\mathbf{x})$ in pseudo colors (cf. Sec. 9.1.3).

Beyerer, Jürgen & León, F.P. & Frese, C.. (2015). Machine vision: Automated visual inspection: Theory, practice and applications.

3D shape capturing

Autofocus sensors

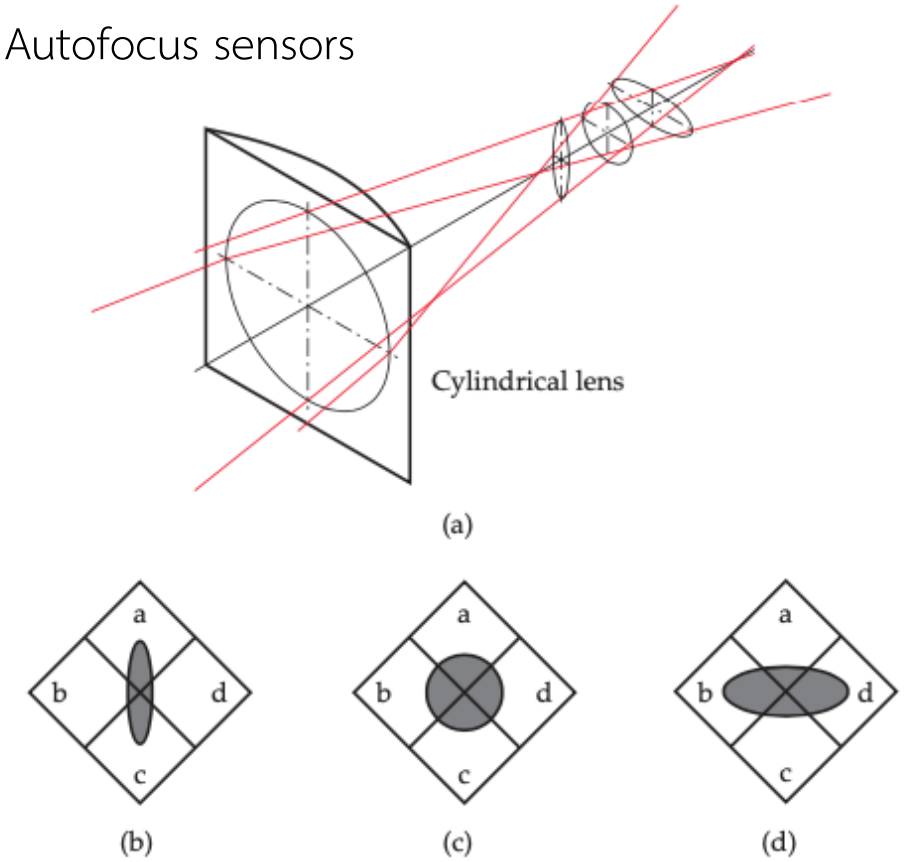

Figure 7.83. Principle of astigmatic focus detection using a cylindrical lens and a 4-quadrant photo detector. (a) Distortion of the ray bundle in the case of a cylindrical lens; (b) Image on a 4-quadrant detector caused by an object distance which is too low; (c) Focused imaging; (d) Distance too large.

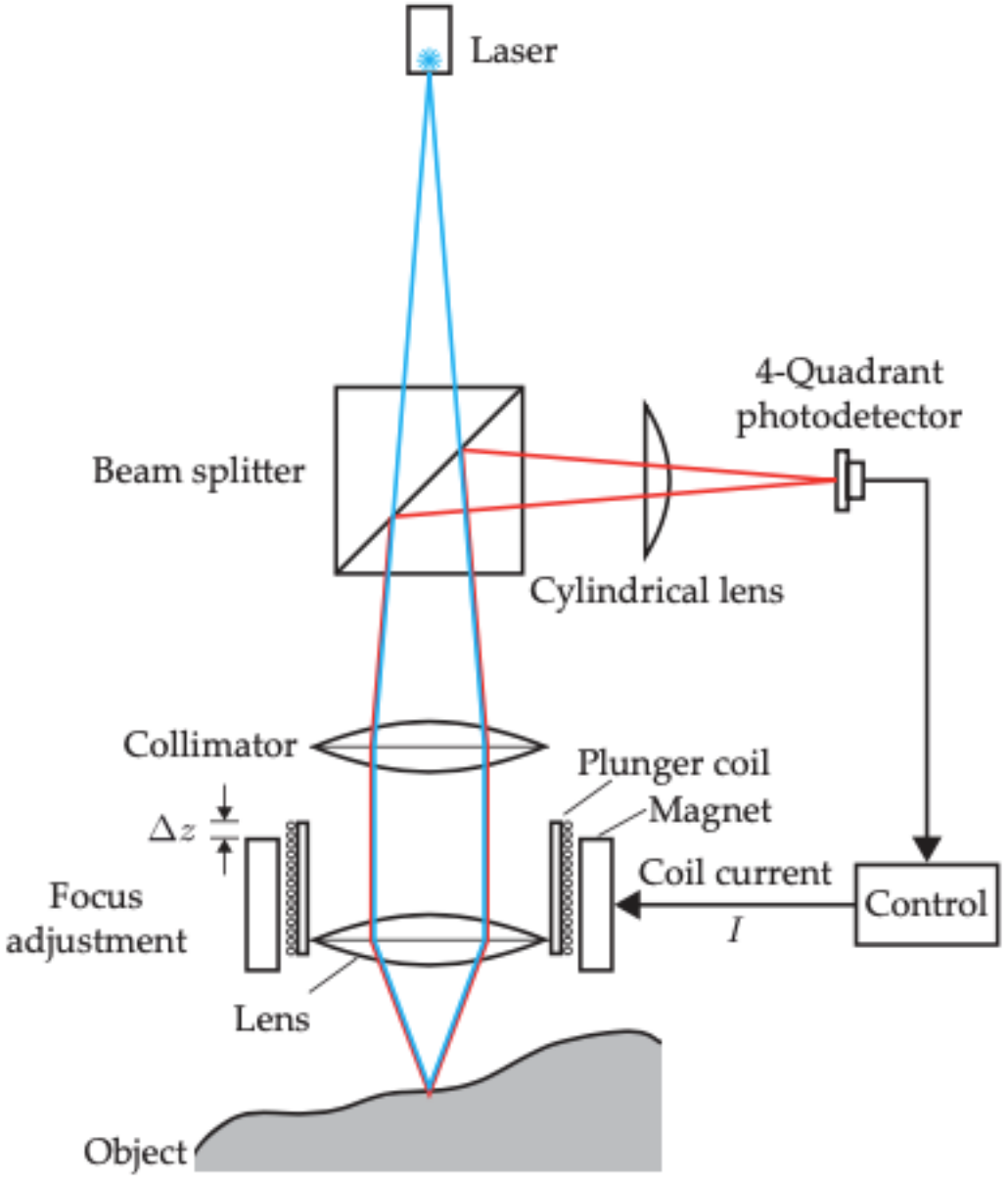

Figure 7.82. Autofocus sensor: Optical path and electromechanic focus correction.

Beyerer, Jürgen & León, F.P. & Frese, C.. (2015). Machine vision: Automated visual inspection: Theory, practice and applications.

3D shape capturing

Confocal microscopy

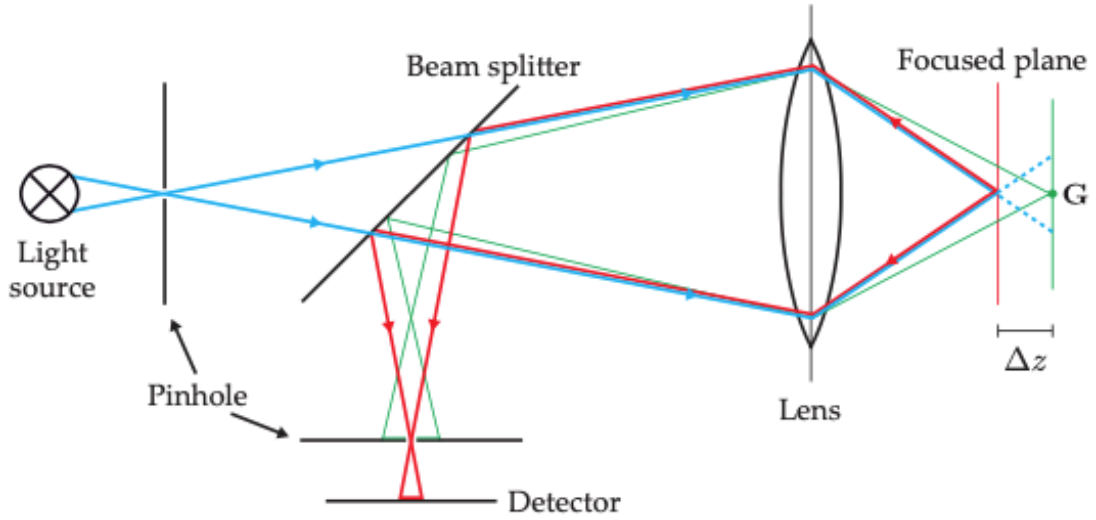

Figure 7.84. Optical path in the case of confocal microscopy. The illumination rays are colored in blue, the optical path of the optical imaging is drawn in red and green. The defocused light bundle, which is colored in green, can hardly pass the diaphragm of the detector.

Beyerer, Jürgen & León, F.P. & Frese, C.. (2015). Machine vision: Automated visual inspection: Theory, practice and applications.

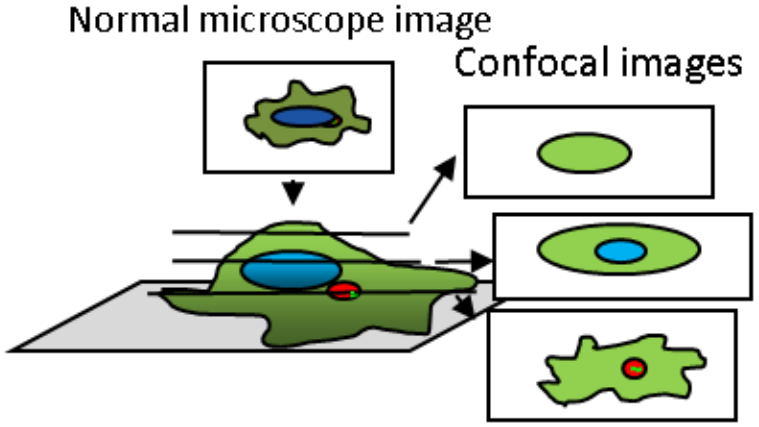

Pictorial showing the difference between a normal microscope view and confocal image

https://www.immunology.org/public-information/bitesized-immunology/experimental-techniques/laser-confocal-microscopy

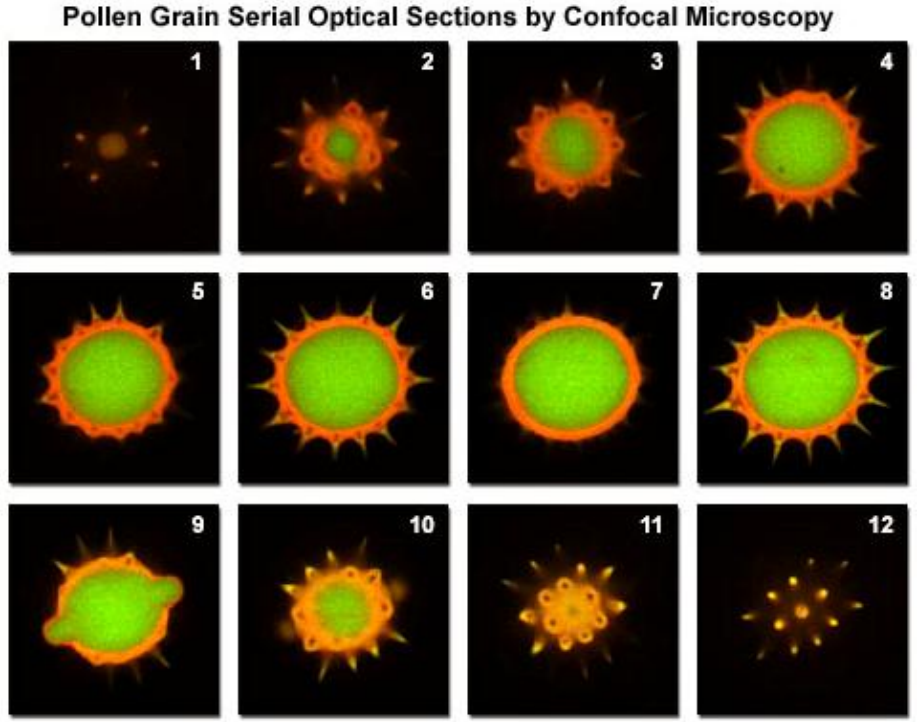

http://www.olympusconfocal.com/theory/confocalintro.html

3D shape capturing

Confocal chromatic triangulation (CCT)

- It combines the principle of a con- focal chromatic microscope with the principle of triangulation.
- The CCT sensor is a line-scan sensor that captures the height z(x, y) of an object's surface in a one-dimensional scanning process.

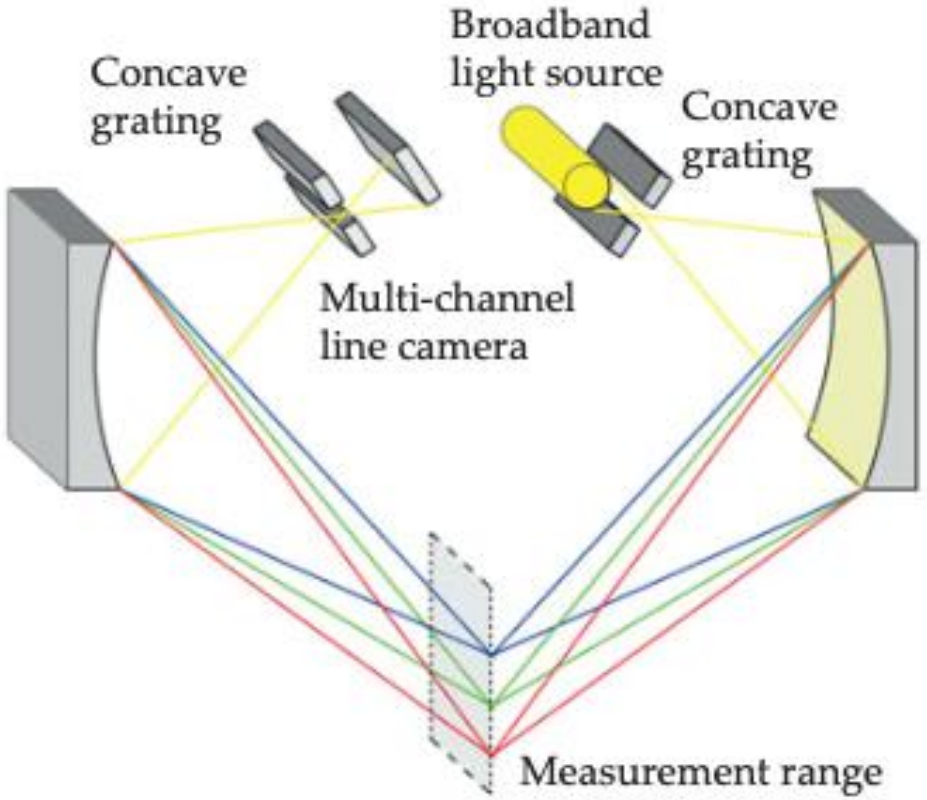

Figure 7.87. Setup principle of a CCT sensor.

Beyerer, Jürgen & León, F.P. & Frese, C.. (2015). Machine vision: Automated visual inspection: Theory, practice and applications.

3D shape capturing

Time-of-flight sensors

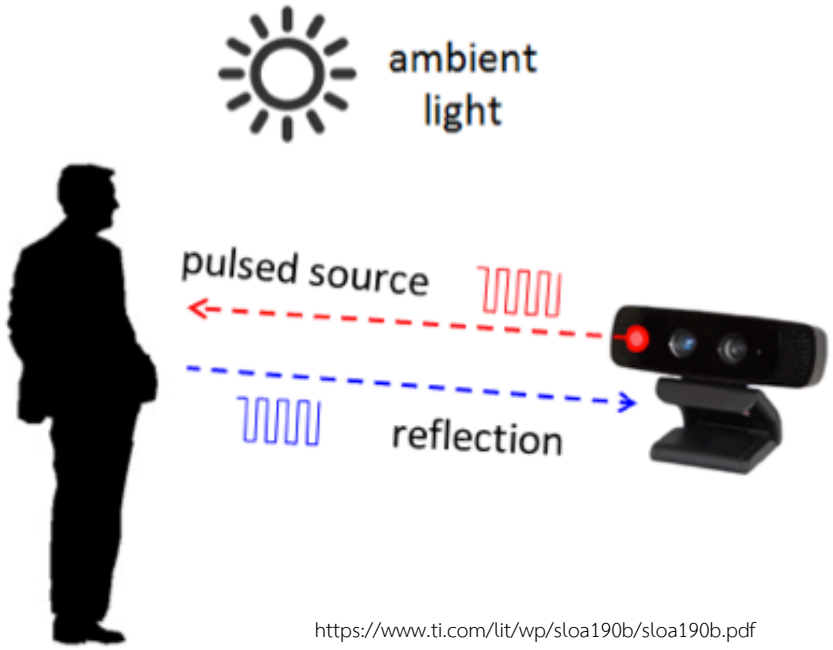

https://www.ti.com/lit/wp/sloa190b/sloa190b.pdf

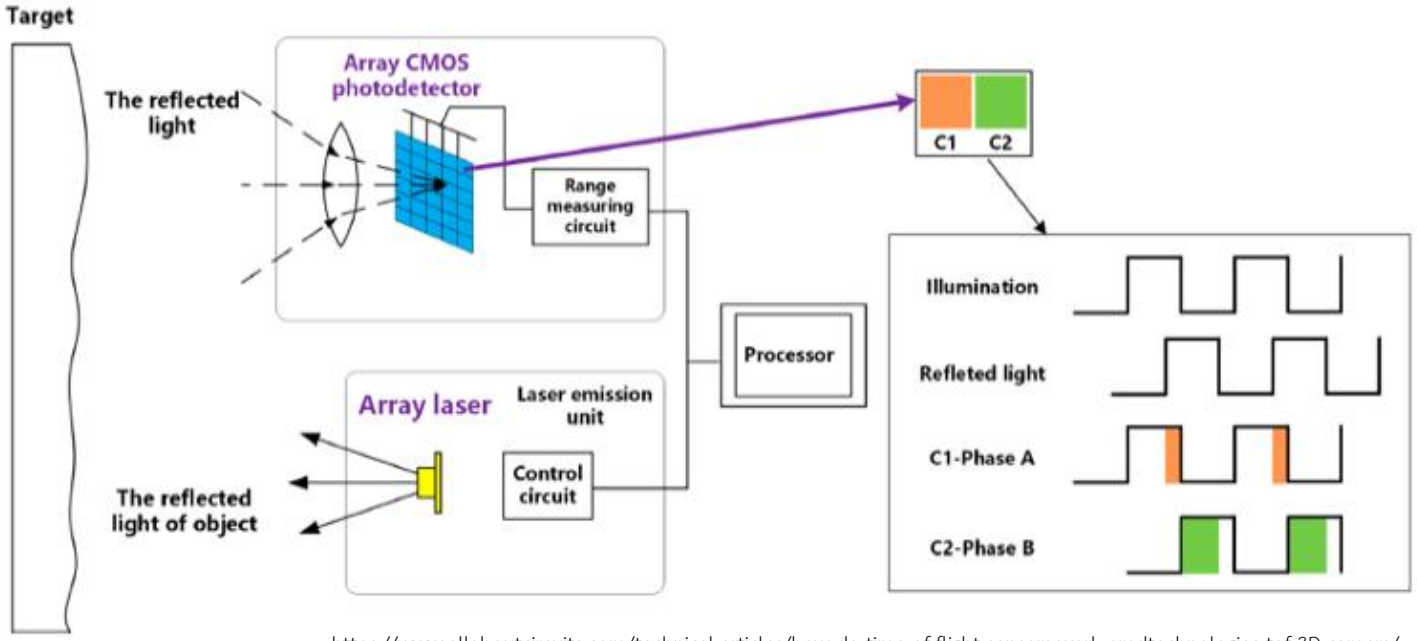

https://www.allaboutcircuits.com/technical-articles/how-do-time-of-flight-sensors-work-pmdtechnologies-tof-3D-camera/

3D shape capturing

Phase-based methods

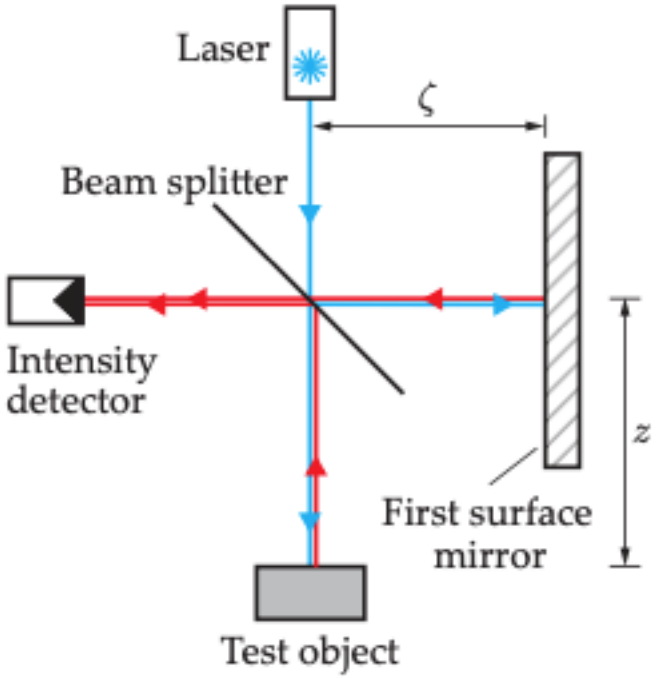

Figure 7.88. Principle of interferometry.

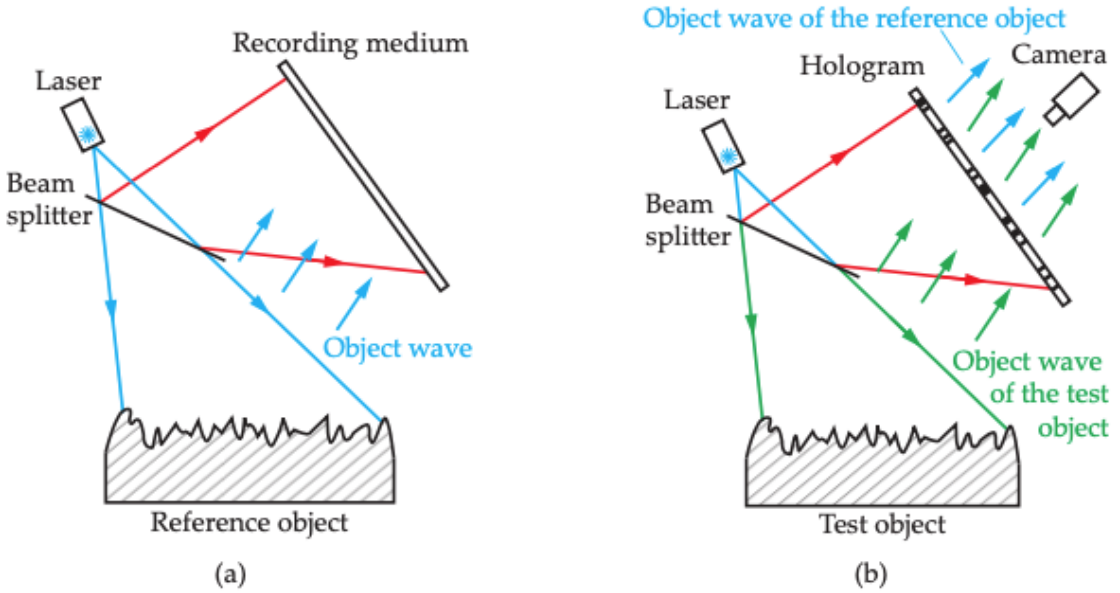

Figure 7.97. Automated visual inspection using holographic interferometry: (a) Recording a hologram of the reference object; (b) Interference of the secondary reference wave (object waves of the reference object) with the object wave of the test object (sketch of the principle).

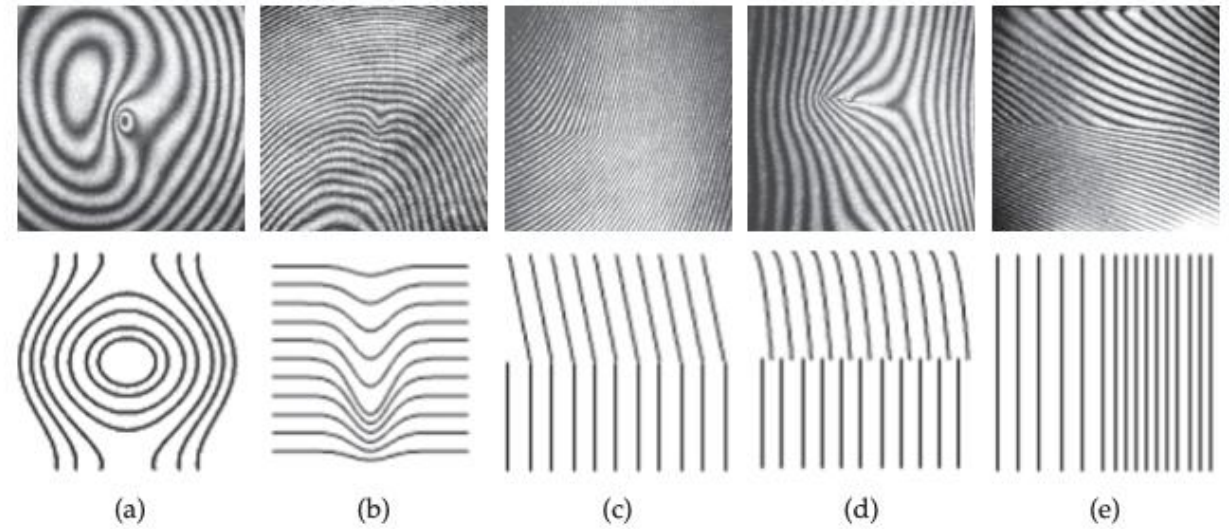

Figure 7.99. Patterns in the hologram corresponding to different types of defects: (a) Bull's eye; (b) Groove; (c) Bend; (d) Displacement; (e) Compression; Upper row: Holographic interference patterns; Lower row: Schematic illustration of the characteristic stripes (source: Prof. Dr. W. Osten [125]).

Beyerer, Jürgen & León, F.P. & Frese, C.. (2015). Machine vision: Automated visual inspection: Theory, practice and applications.

3D shape capturing

- Photoelasticity

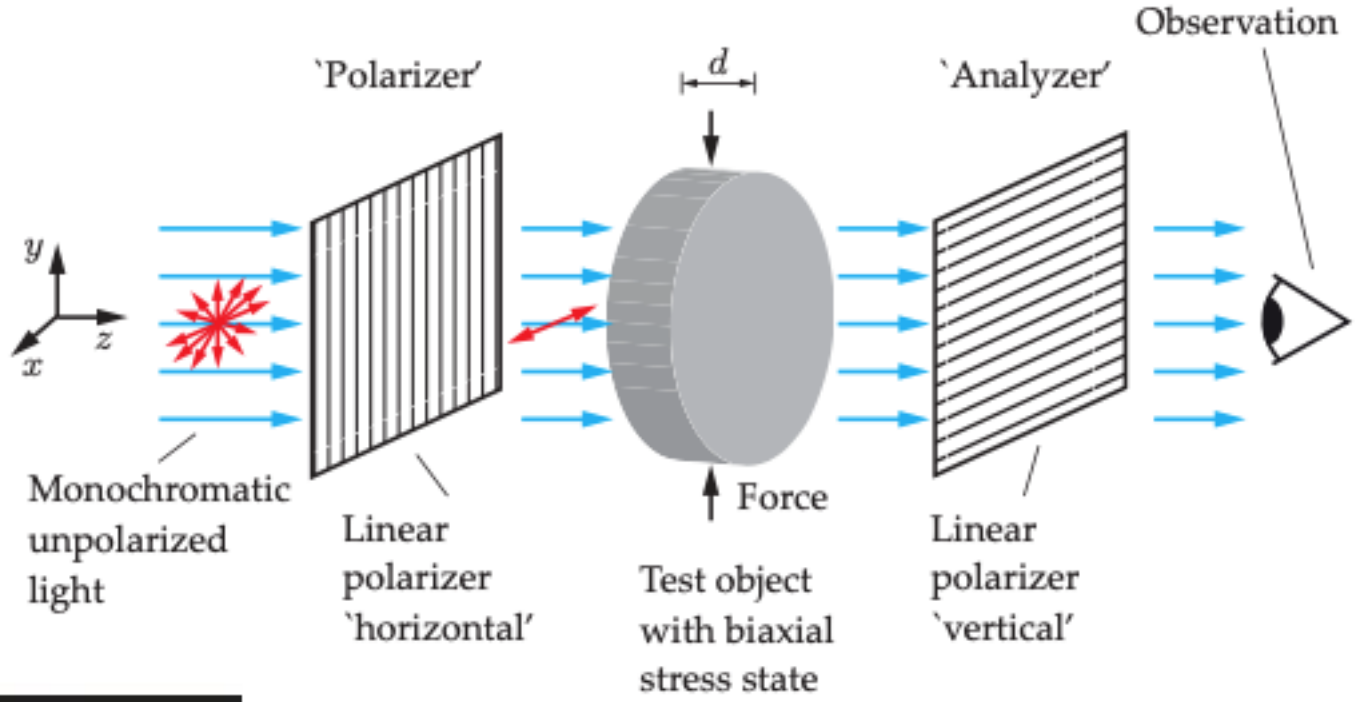

Figure 7.114. Polariscope with crossed linear polarizers.

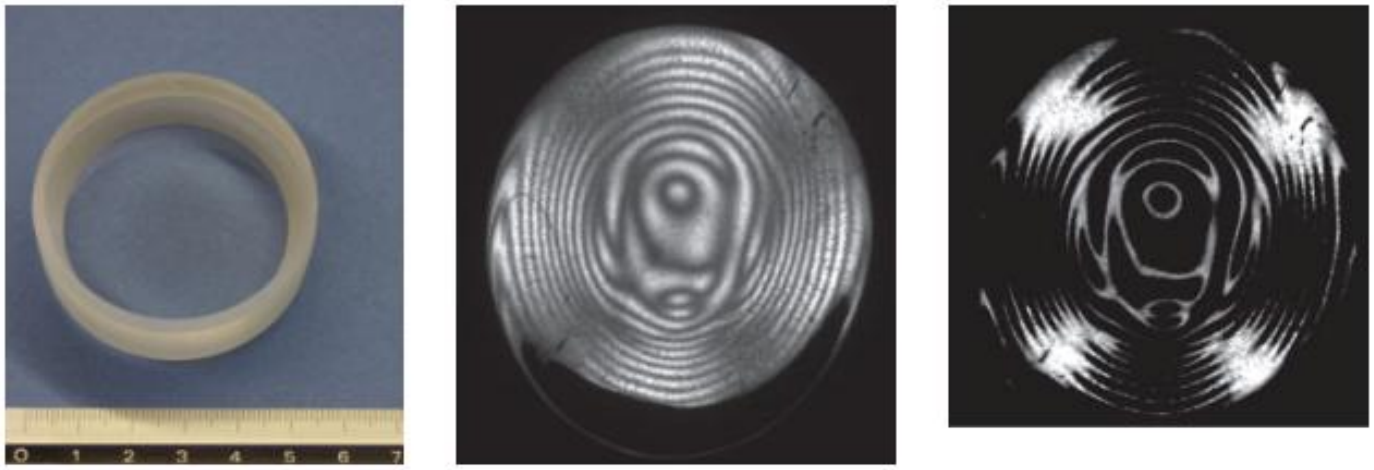

(a) (b) (c)

Figure 7.115. Inspection of a lens blank using photoelasticity: (a) Photograph of the test object together with a cm scale in order to visualize the dimensions; (b) Total intensity of a photoelasticity image; (c) Photoelasticity images for crossed polarizers.

Beyerer, Jürgen & León, F.P. & Frese, C.. (2015). Machine vision: Automated visual inspection: Theory, practice and applications.

Special image acquisition methods

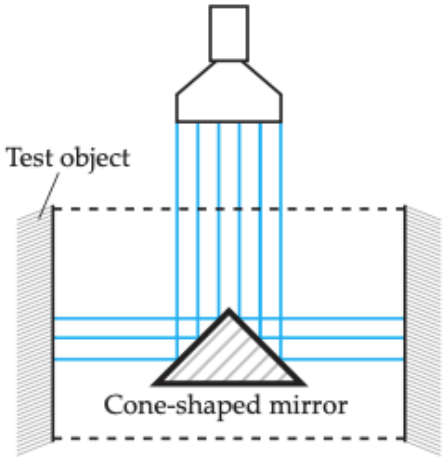

Inspection of cylindrical and radial structures using a cone-shaped mirror.

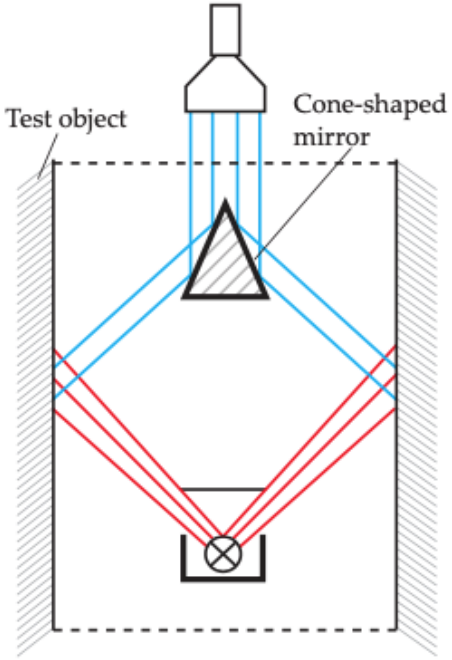

Inspection of drill holes using a cone-shaped mirror and bright-field illumination.

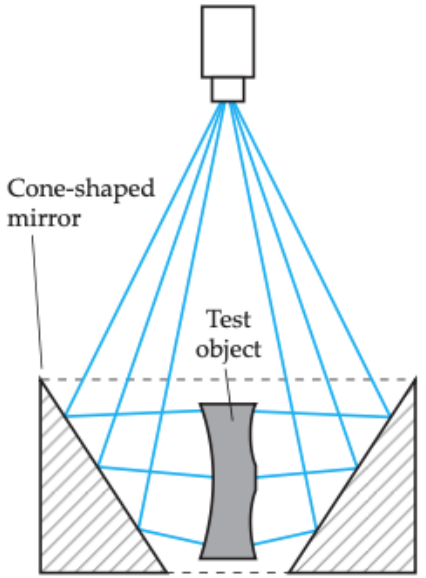

Radial inspection of the object's outside using a cone shaped mirror.

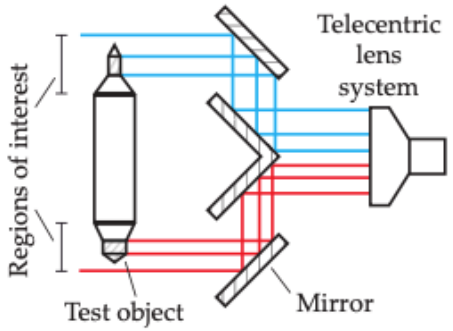

Telecentric measurement and inspection of specific object regions using a suitable setup of mirrors.

Beyerer, Jürgen & León, F.P. & Frese, C.. (2015). Machine vision: Automated visual inspection: Theory, practice and applications.

Special image acquisition methods

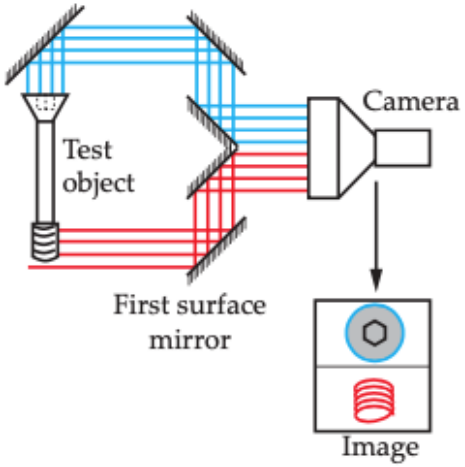

Inspection of specific regions on different sides of the test object by means of a special setup of mirrors.

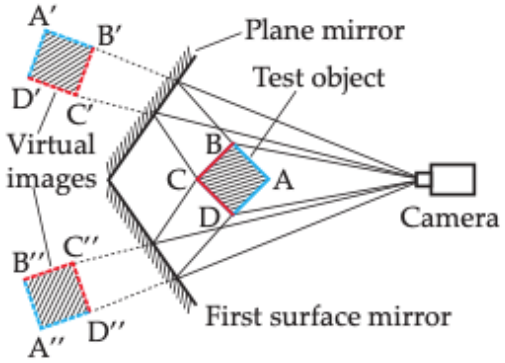

Inspection of all sides of a test object using mirrors. Two planar mirrors are placed behind the test object, so that its back can be imaged by the camera. Therefore, the complete perimeter of the object can be captured.

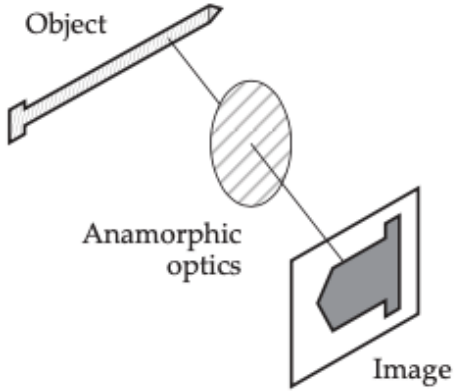

Anamorphic imaging system consisting of several lenses, including a cylindrical lens. An anamorphic optics has different magnifications in the x- and y-directions, and thus long objects can be almost completely captured. Such an optic can be realized with two cylindrical lenses which are rotated by $90°$ with respect to each other [145].

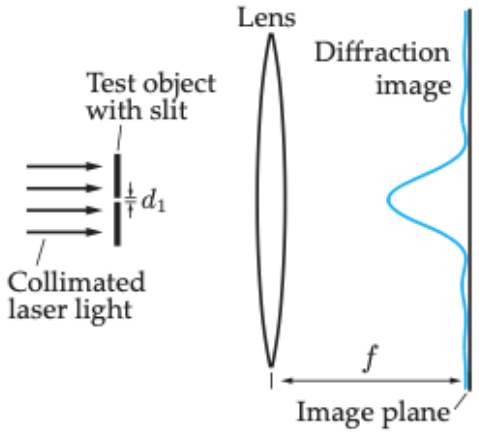

Measurement of narrow slits by inspecting the diffraction image. The distances between the extrema are reciprocal to the slit width d_1.

Beyerer, Jürgen & León, F.P. & Frese, C.. (2015). Machine vision: Automated visual inspection: Theory, practice and applications.

Special image acquisition methods

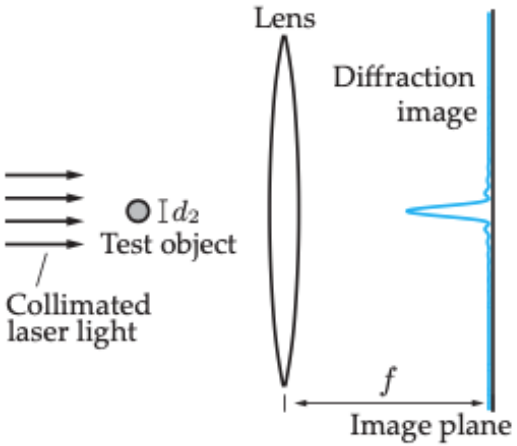

Measurement of the diameter d_2 of cylindrical objects. In accordance with Babinet's principle, a slit and a diaphragm shaped as the slit's complement produce the same diffraction image (see Sec. 2.2.6). Here, the diffraction image is smaller than in the previous example, because $d_1 < d_2$.

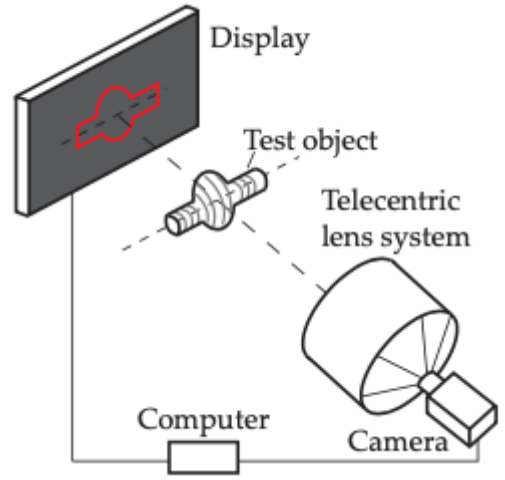

Quasi-telecentric illumination using a monitor which brightly displays the slightly expanded contour of the test object and is black apart from that. This prevents systematic measurement errors caused by a non-telecentric background illumination and is much more inexpensive for large lenses than a telecentric illumination (cf. Sec. 7.3.10.2).

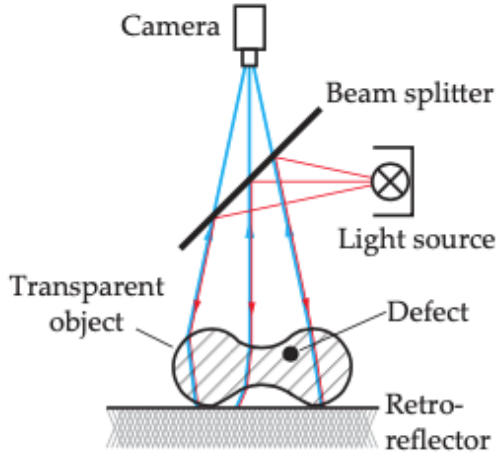

Inspection of transparent test objects. The influence of refraction is suppressed by means of a retroreflector, as the light uses the same optical path towards and away from the reflector. This leads to images with almost homogeneous intensity [69].

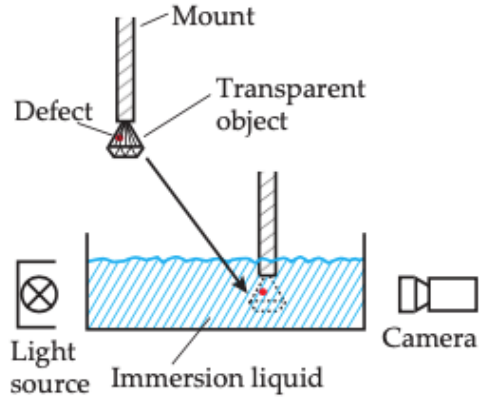

Inspection of transparent test objects. The test object is made invisible with respect to refraction by placing it in an immersion bath of a liquid having an index of refraction equal to that of the test object. Only inner defects remain visible.

Beyerer, Jürgen & León, F.P. & Frese, C.. (2015). Machine vision: Automated visual inspection: Theory, practice and applications.

Special image acquisition methods

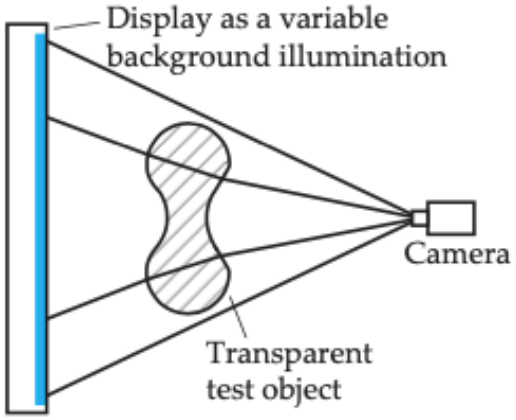

Inspection of transparent or partially transparent objects with variable background illumination using a display.

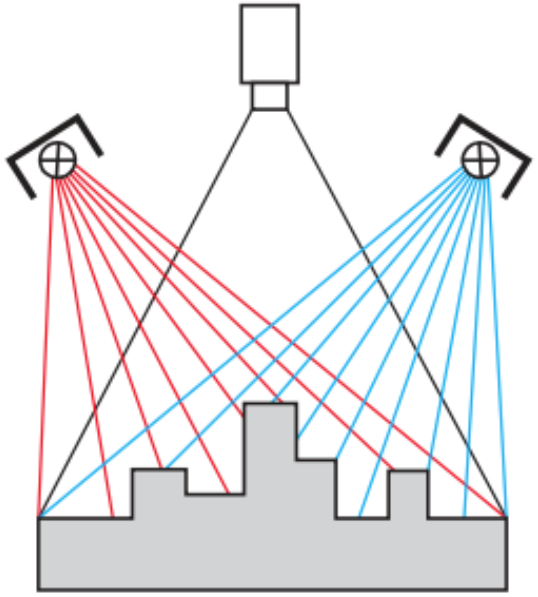

Together, N light sources with different illumination directions illuminate the test object and generate an image series with different shadows. The image series can be obtained by sequentially capturing several images, or by using different colors for the different illumination directions [21, 22, 75]. The shadows contain the implicit 3D information. The comparison with reference images allows a robust detection of break-offs and other 3D defects.

Beyerer, Jürgen & León, F.P. & Frese, C.. (2015). Machine vision: Automated visual inspection: Theory, practice and applications.

Universal principles

Suppression of extraneous light

- Isolation
- Modulation
- High signal-to-noise ratio
- Narrow-band illumination
- Reference image

Beyerer, Jürgen & León, F.P. & Frese, C.. (2015). Machine vision: Automated visual inspection: Theory, practice and applications.

Universal principles

Inverse illumination

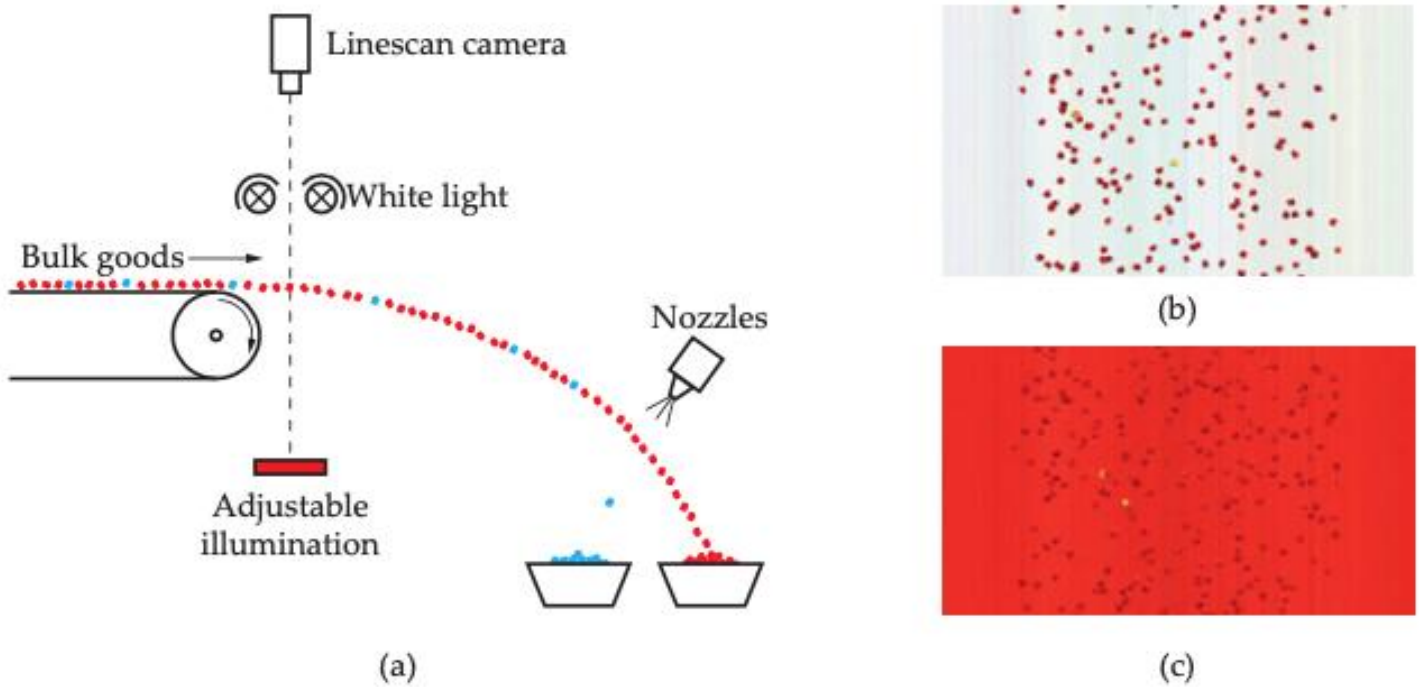

Figure 7.120. Inverse illumination for sorting bulk goods: (a) Sorting site with inverse illumination; (b) White light image of plastic granulates without adjusted background; (c) Image with inverse background illumination.

Beyerer, Jürgen & León, F.P. & Frese, C.. (2015). Machine vision: Automated visual inspection: Theory, practice and applications.

Universal principles

Inverse illumination

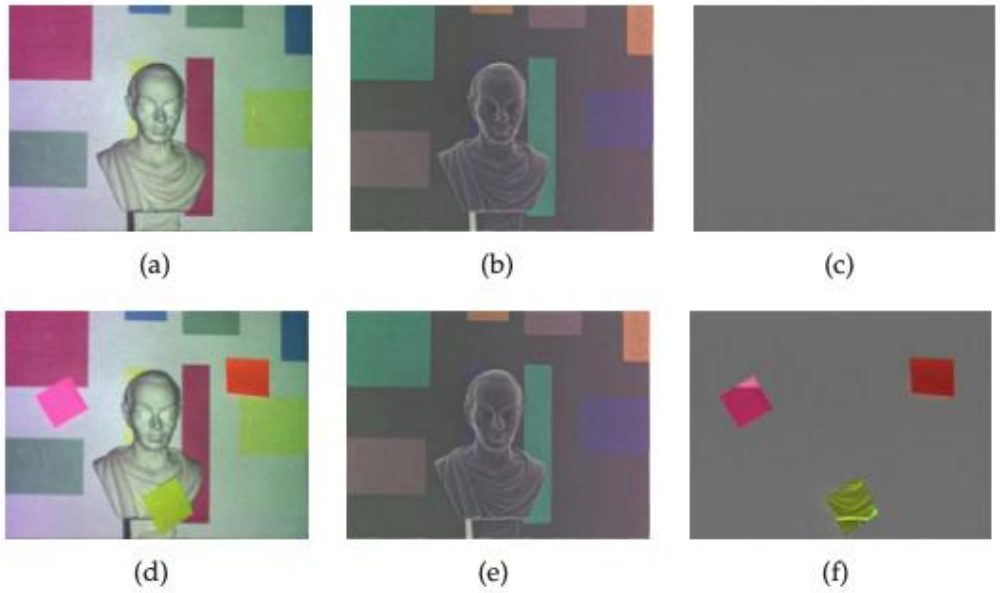

Figure 7.122. Examples of variable inverse illumination using the setup of Fig. 7.121: (a) Scene; (b) Projected inverse illumination; (c) Camera image; (d) Modified scene; (e) Projected inverse illumination (identical to (b)); (f) Corresponding camera image.

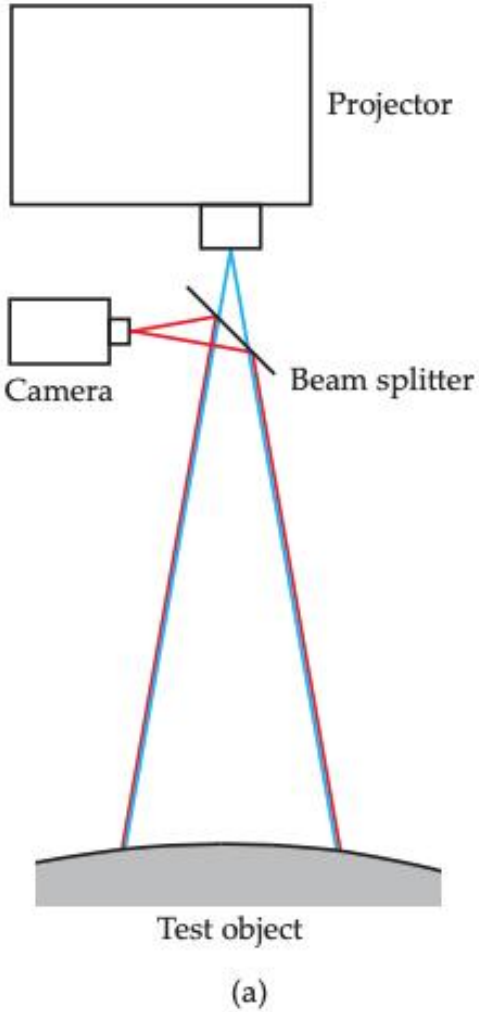

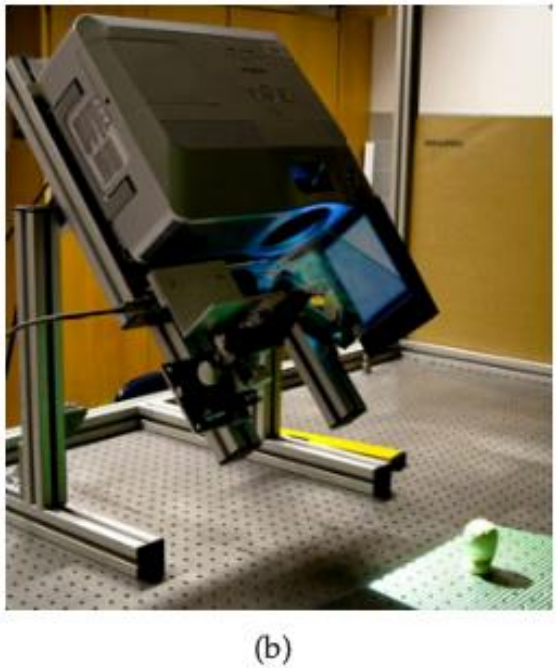

Figure 7.121. Setup for variable, coaxial inverse illumination.

Beyerer, Jürgen & León, F.P. & Frese, C.. (2015). Machine vision: Automated visual inspection: Theory, practice and applications.

Universal principles

Inverse illumination

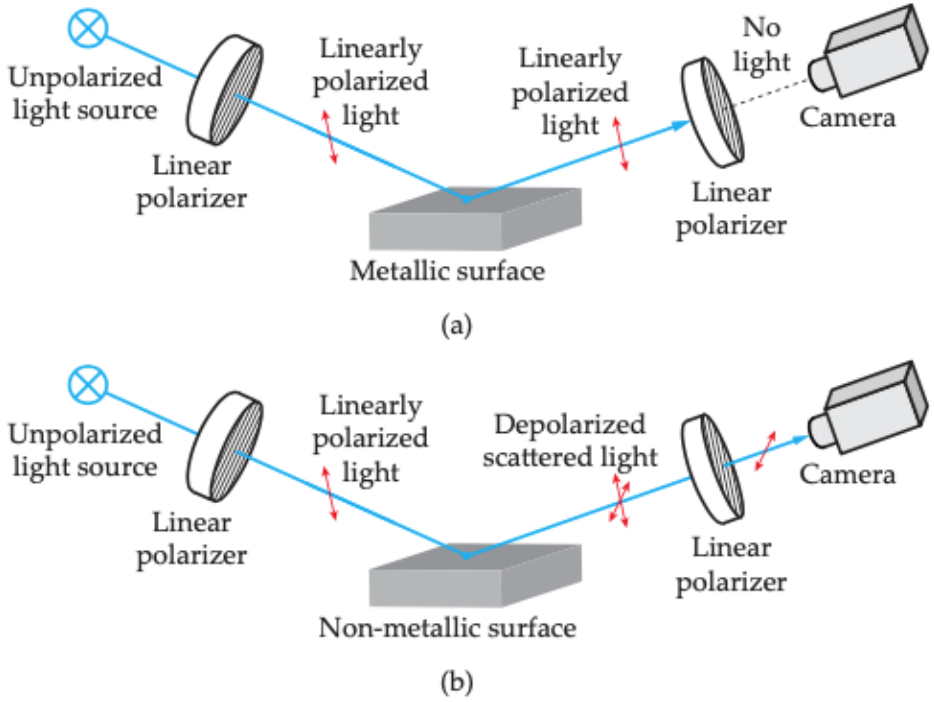

Figure 7.123. Discrimination of metals from non-metals by using polarization effects: (a) Linearly polarized light remains linearly polarized after being reflected by the surface of a metal and is therefore blocked by a crossed polarizer; (b) Non-metals partially depolarize the reflected light, so that it can partly pass the crossed polarizer.

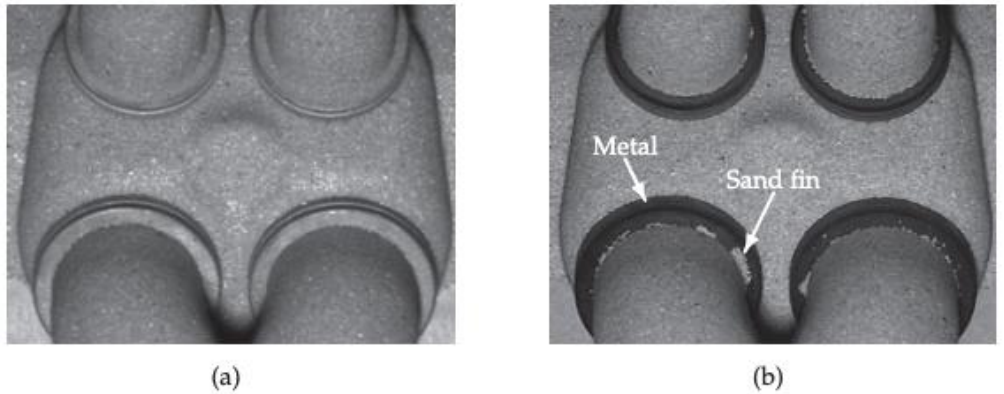

Figure 7.124. Polarized illumination for the detection of sand fins in the sand cores of combustion chambers: (a) Images acquired using unpolarized light; (b) Images acquired with linearly polarized illumination, observed through a polarizer crossed to the reflected light.

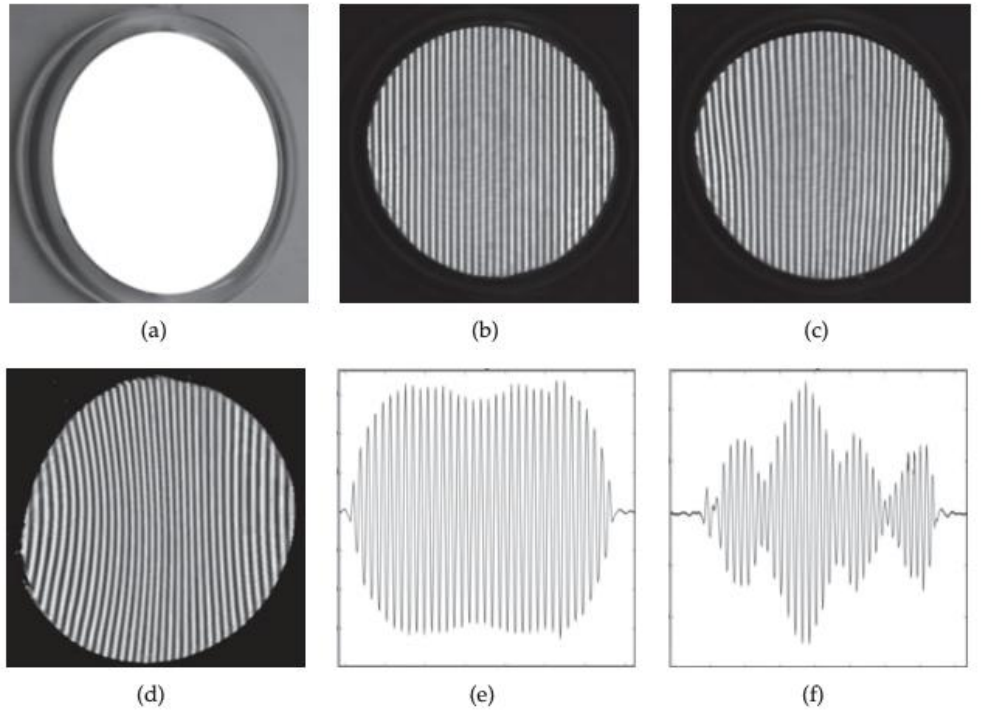

Figure 7.125. Inverse pattern for the deflectometric inspection of a magnifying mirror: (a) Reference object; (b) Deflectometric image of the intact reference object; (c) Deflectometric image of a deformed object, here, an arched mirror; (d) Inverse pattern displayed by the pattern generator; (e) Evaluation for the reference object, vertical projection of (b); (f) Evaluation for the deformed object, vertical projection of (c).

Beyerer, Jürgen & León, F.P. & Frese, C.. (2015). Machine vision: Automated visual inspection: Theory, practice and applications.

Image Signals

Mathematical model of image signals

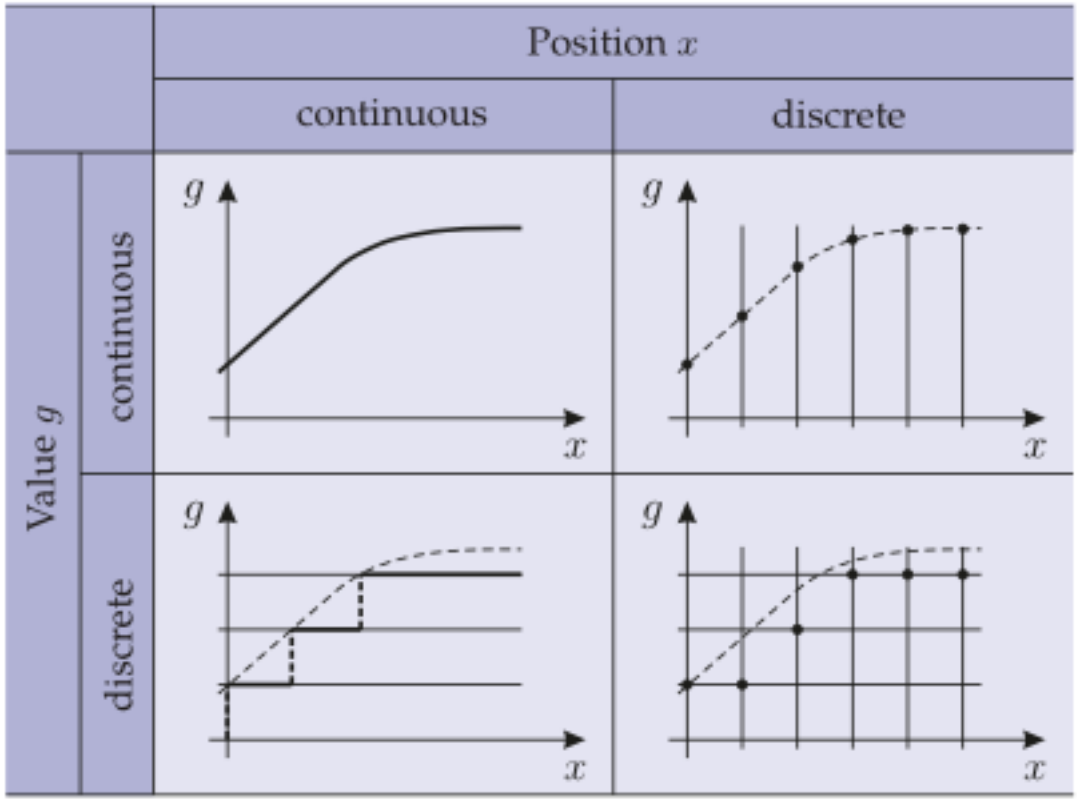

Figure 8.1. Discretization of position and function values.

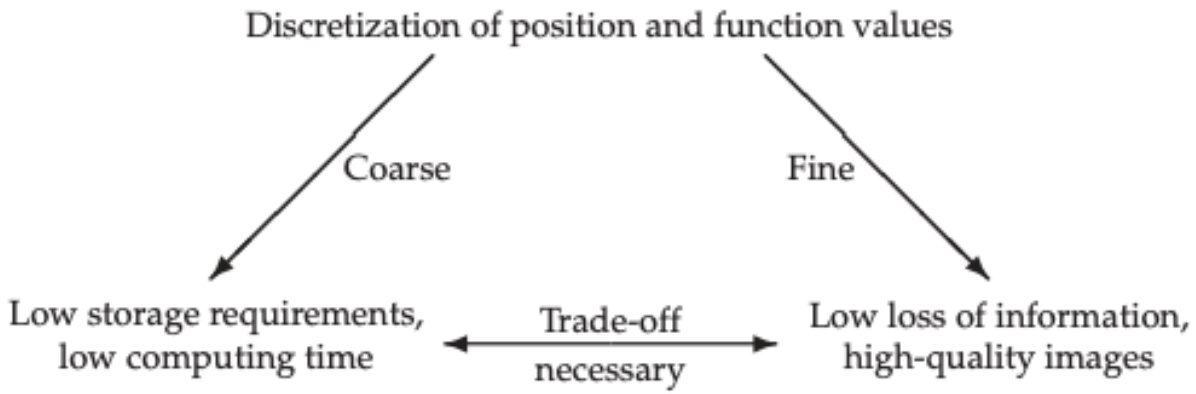

Figure 8.2. Consequences of the discretization of position and function values.

Beyerer, Jürgen & León, F.P. & Frese, C.. (2015). Machine vision: Automated visual inspection: Theory, practice and applications.

Image Signals

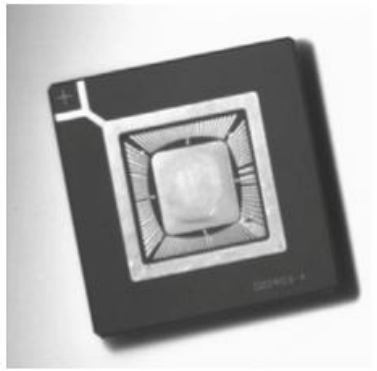

(a) 256×256

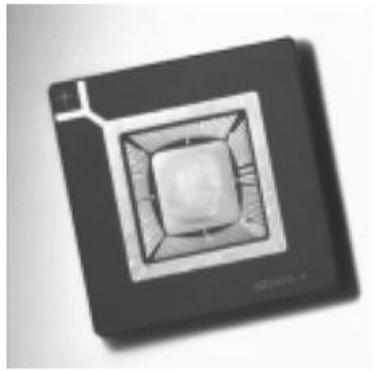

(b) 128×128

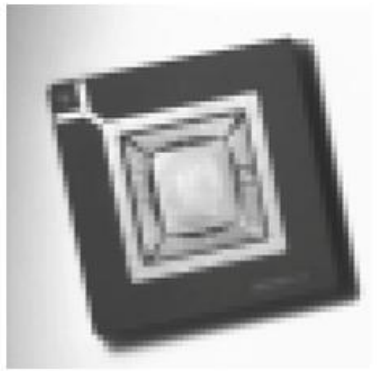

(c) 64×64

(d) 32×32

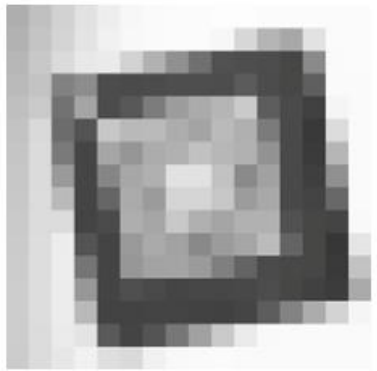

(e) 16×16

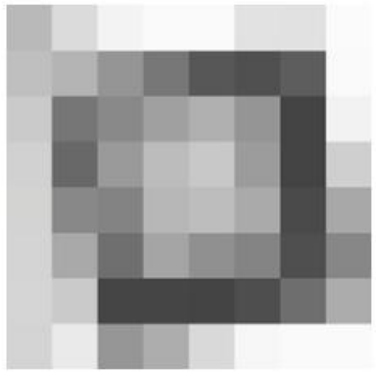

(f) 8×8

Figure 8.3. Spatial discretization: Test image with different spatial resolutions.

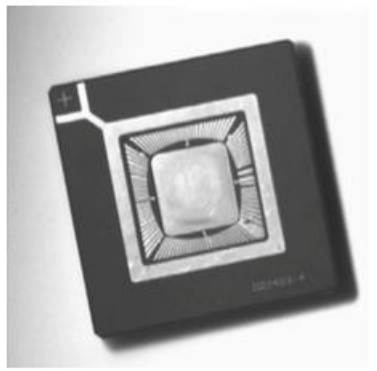

(a) 64 Gray values

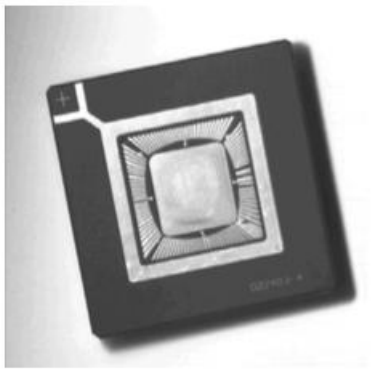

(b) 32 Gray values

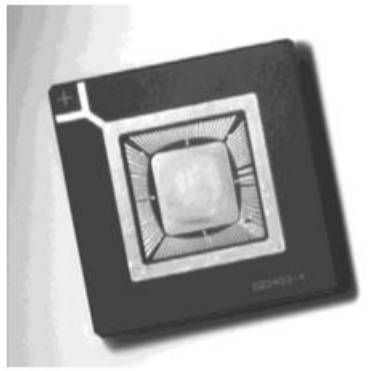

(c) 16 Gray values

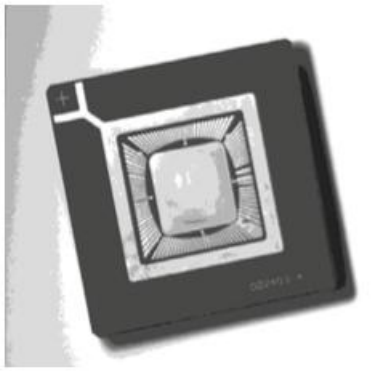

(d) 8 Gray values

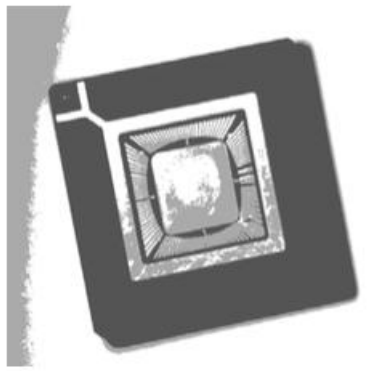

(e) 4 Gray values

(f) 2 Gray values

Figure 8.4. Discretization of function values: Test image with different resolutions of gray values.

Beyerer, Jürgen & León, F.P. & Frese, C.. (2015). Machine vision: Automated visual inspection: Theory, practice and applications.

Image Signals

- Color spaces

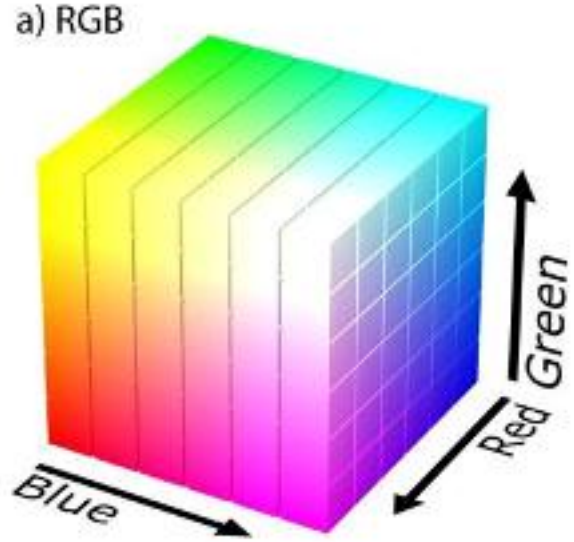

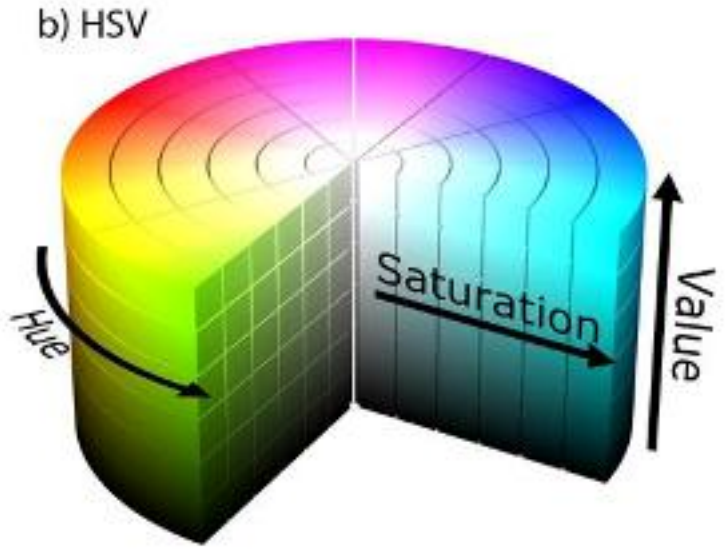

Image Processing

Preprocessing

- It carried out to improve the quality of the image and emphasize the features required by the application.

TABLE 5.1

Common Image Preprocessing Operations

Preprocessing for	Filtering	Subsampling/ Scaling	Histogram Generation
Illumination rectifications	√	√	√
Blur and focus rectifications	√	√	√
Noise removal	√	√	√
Thresholding			√
Edge enhancements	√	√	√
Segmentation		√	√
Region processing and filters	√	√	√
Color space conversions		√	√

Anand, Sheila & Loganathan, Priya. (2019). A Guide for Machine Vision in Quality Control.

Image Processing

Filtering

- It is a technique that is used to modify or enhance an image.
- Image processing operations implemented with filtering include smoothing, sharpening, and edge enhancement.

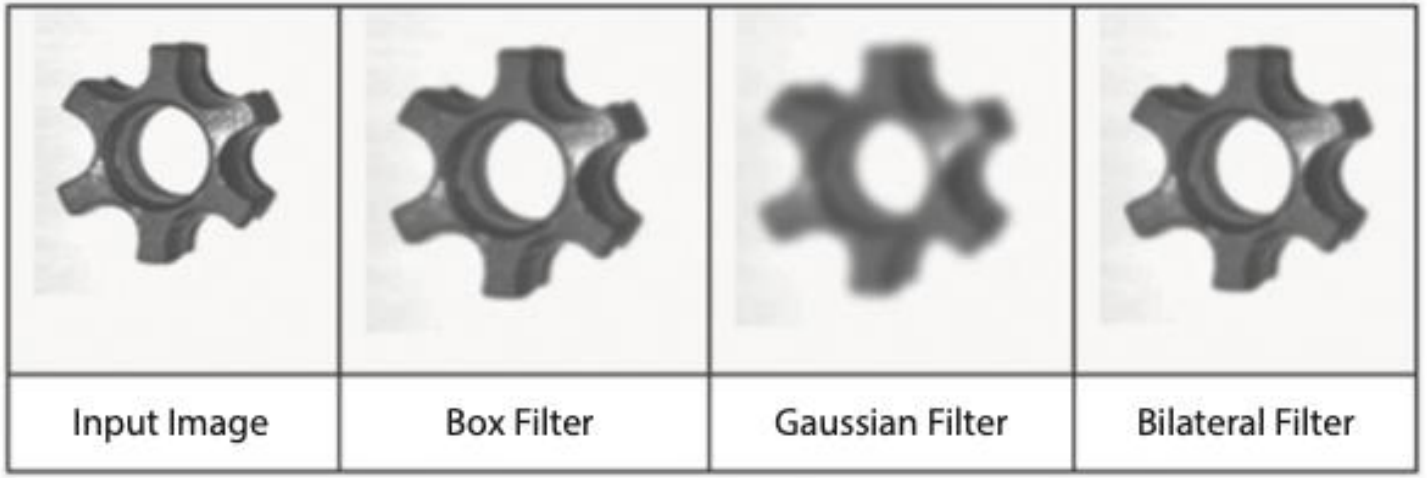

FIGURE 5.2
Sample images obtained from different filtering techniques.

Anand, Sheila & Loganathan, Priya. (2019). A Guide for Machine Vision in Quality Control.

Image Processing

Subsampling/Scaling

FIGURE 5.3
Images obtained with bilinear and nearest-neighbor interpolation.

Anand, Sheila & Loganathan, Priya. (2019). A Guide for Machine Vision in Quality Control.

Image Processing

Histogram

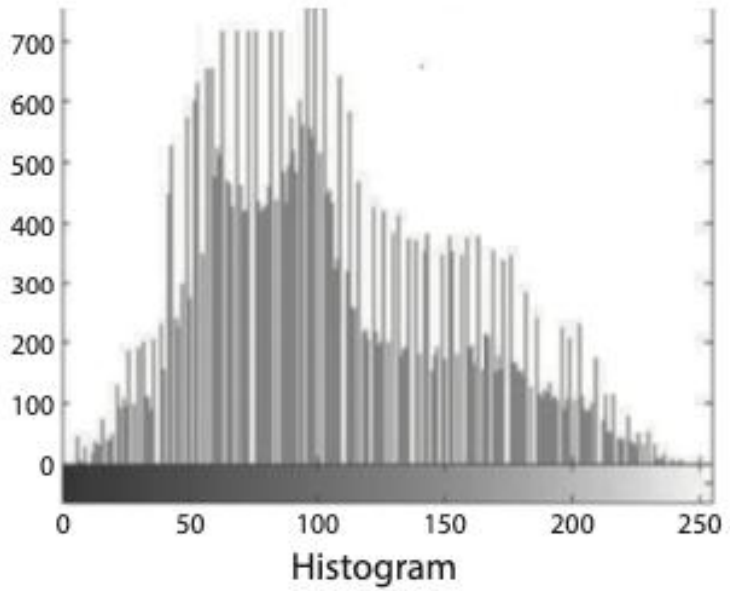

FIGURE 5.4
Image of a neck bone and histogram.

Anand, Sheila & Loganathan, Priya. (2019). A Guide for Machine Vision in Quality Control.

Image Processing

Image Segmentation

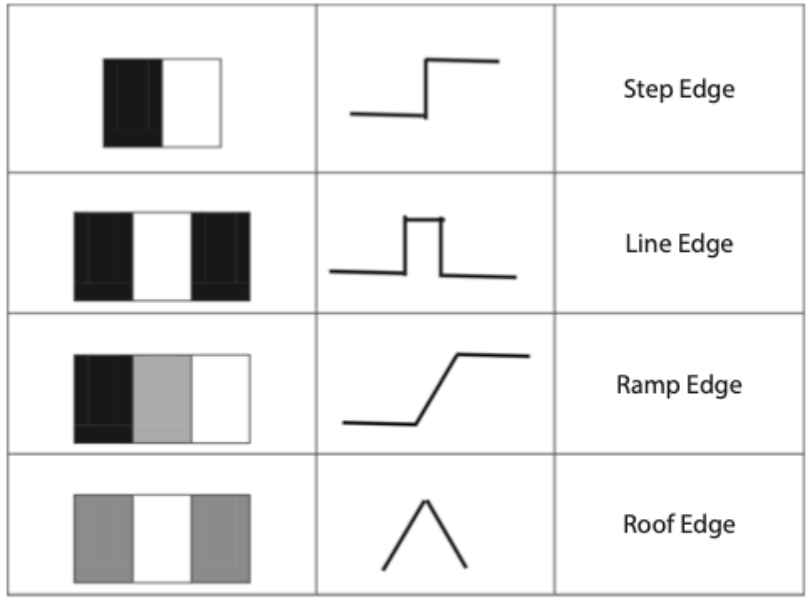

FIGURE 5.6
Different types of edges in a digital image.

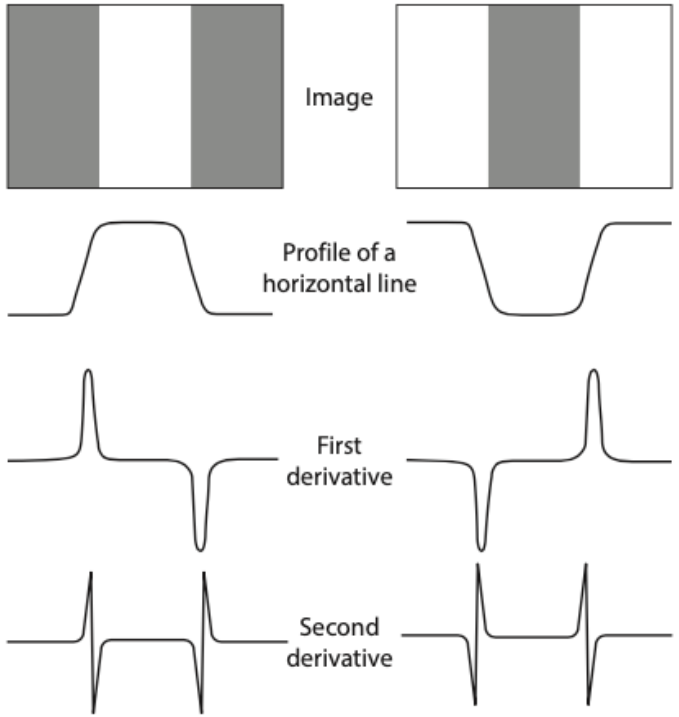

FIGURE 5.7
First- and second-order derivatives.

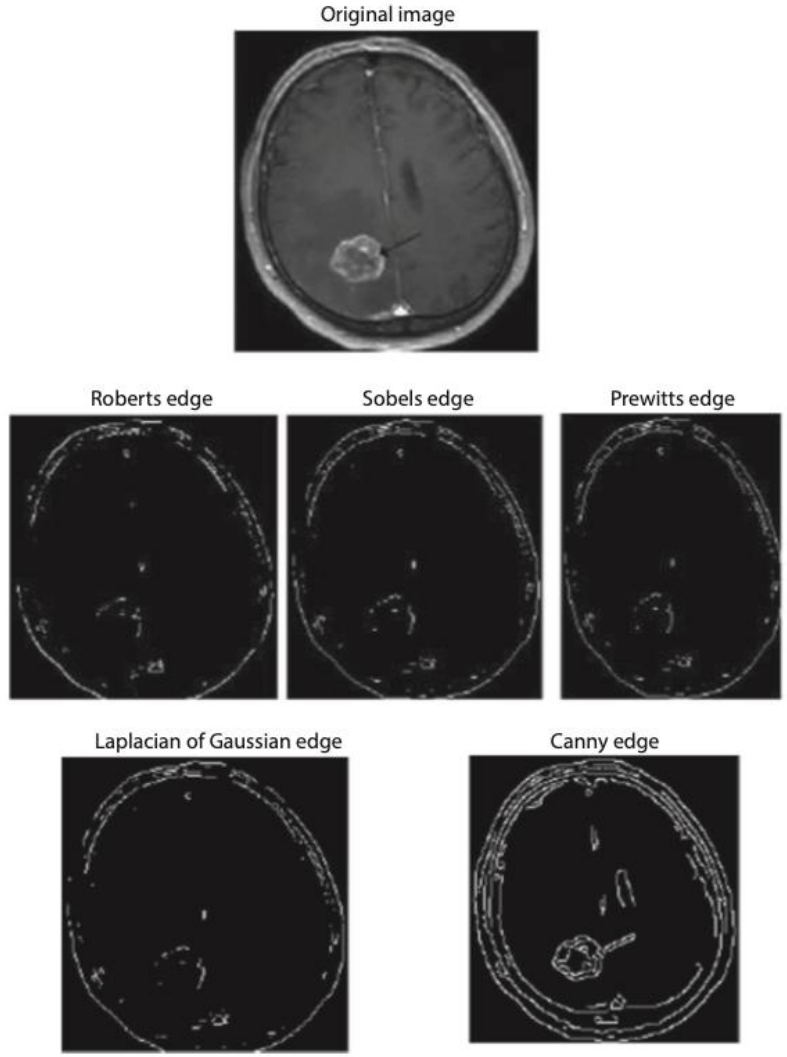

FIGURE 5.12
Results of various edge detection methodologies.

Anand, Sheila & Loganathan, Priya. (2019). A Guide for Machine Vision in Quality Control.

Machine Vision Application in Quality Control

Key benefits of using machine vision

- Accuracy
- Speed
- Repeatability
- 100% Inspection
- Cost

Designing a Machine Vision System

Key questions

- What parts or products have to be inspected?
- Are the inspections continuous (100%) or discrete (sampling)?
- What should be the speed of inspection?
- What are the performance requirements?

The major advantages of this kind of inspection

- Reduction in end-line defects
- Saving in time and effort in final inspection
- Problems can be fixed at the beginning with resulting saving in cost of rework
- Prevention of common mistakes or mistakes that are often repeated

Categorization of Machine Vision Solutions

- Dimensional measurements
- Presence/absence
- Character inspection (OCR, barcode)
- Profile inspection
- Surface inspection
- Robotic guidance

Categorization of Machine Vision Solutions

Dimensional measurements

- Measuring the length and breadth of parts/objects
- Measuring the diameter of circular objects
- Measuring the angle at the edges of objects
- Measuring the position of labels or characters
- Measuring the width of parts/sheets/films

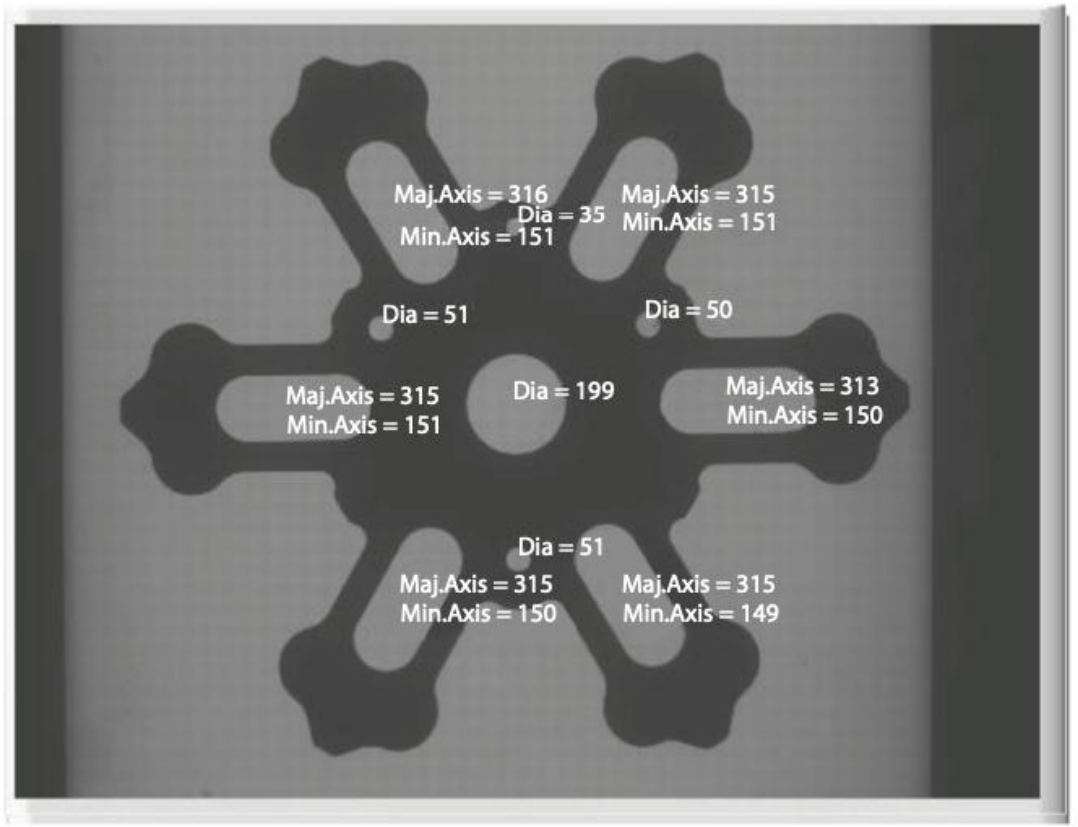

FIGURE 4.3
Dimensional measurement—reed valve.

Anand, Sheila & Loganathan, Priya. (2019). A Guide for Machine Vision in Quality Control.

Categorization of Machine Vision Solutions

Presence/absence

- Checking for the presence of screws and washers used for securing different parts
- Checking for the presence/absence of tablets
- Checking for the completeness of tablets packaging
- Checking for the presence of screws and washers used for securing different parts
- Checking for the presence/absence of tablets
- Checking for the completeness of tablets packaging

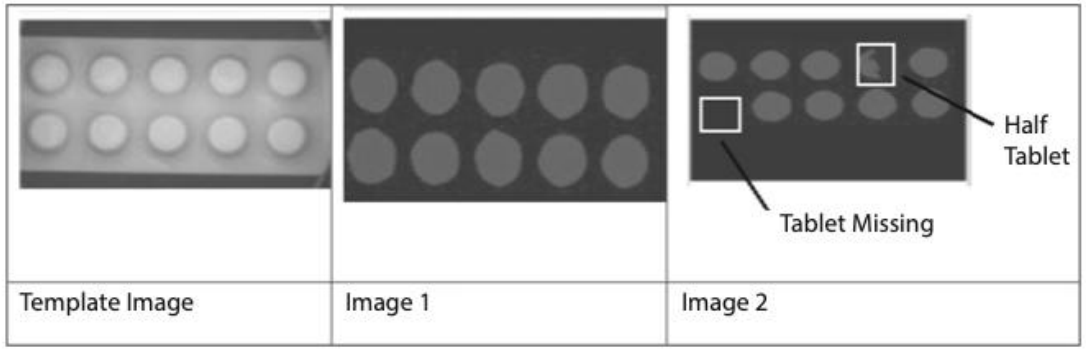

FIGURE 4.4
Presence/absence inspection of a blister pack.

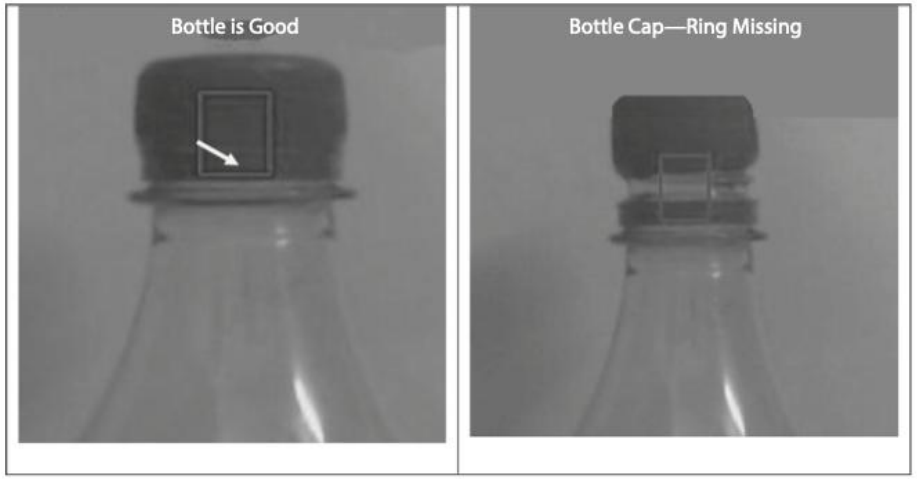

FIGURE 4.5
Presence/absence inspection of a bottle cap.

Anand, Sheila & Loganathan, Priya. (2019). A Guide for Machine Vision in Quality Control.

Categorization of Machine Vision Solutions

Character inspection (OCR, barcode)

(a) (b)

FIGURE 4.6
Sample images of (a) barcode and (b) QR code.

FIGURE 4.7
Sample image for label and barcode inspection.

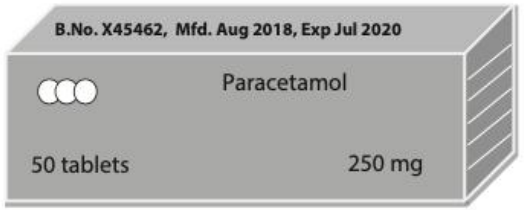

FIGURE 4.8
Sample image for drug pack inspection.

Anand, Sheila & Loganathan, Priya. (2019). A Guide for Machine Vision in Quality Control.

Categorization of Machine Vision Solutions

Profile inspection

FIGURE 4.12
Profile inspection—checking bottle fill levels.

Image taken using frontlighting

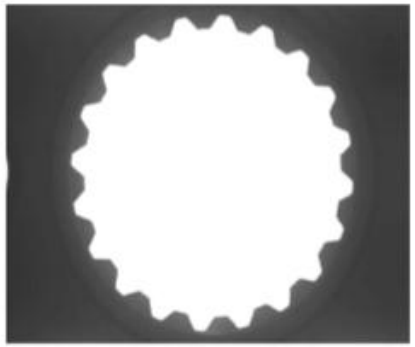

Image taken using backlighting

FIGURE 4.10
Spline gear inspection—images of sample spline gear.

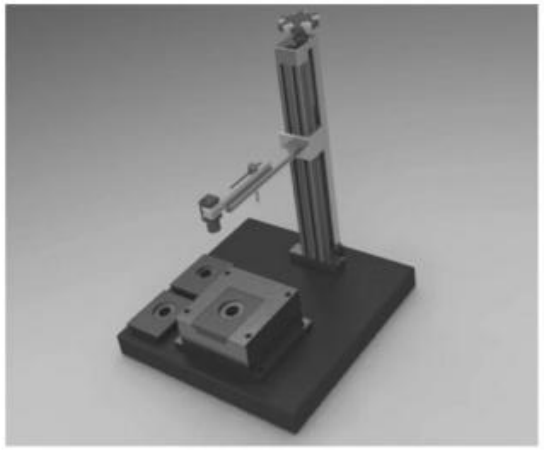

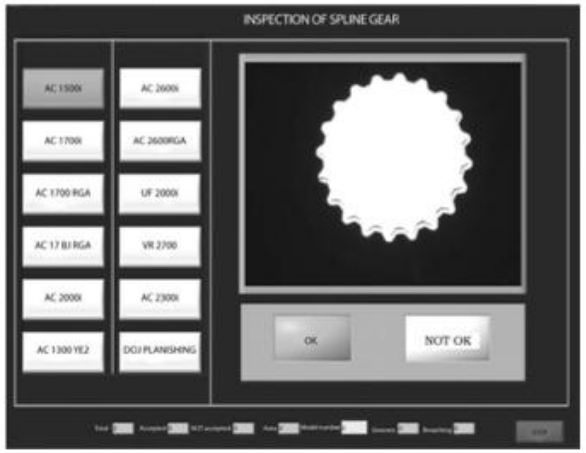

FIGURE 4.11
Spline gear inspection—machine vision setup.

Anand, Sheila & Loganathan, Priya. (2019). A Guide for Machine Vision in Quality Control.

Categorization of Machine Vision Solutions

Surface inspection

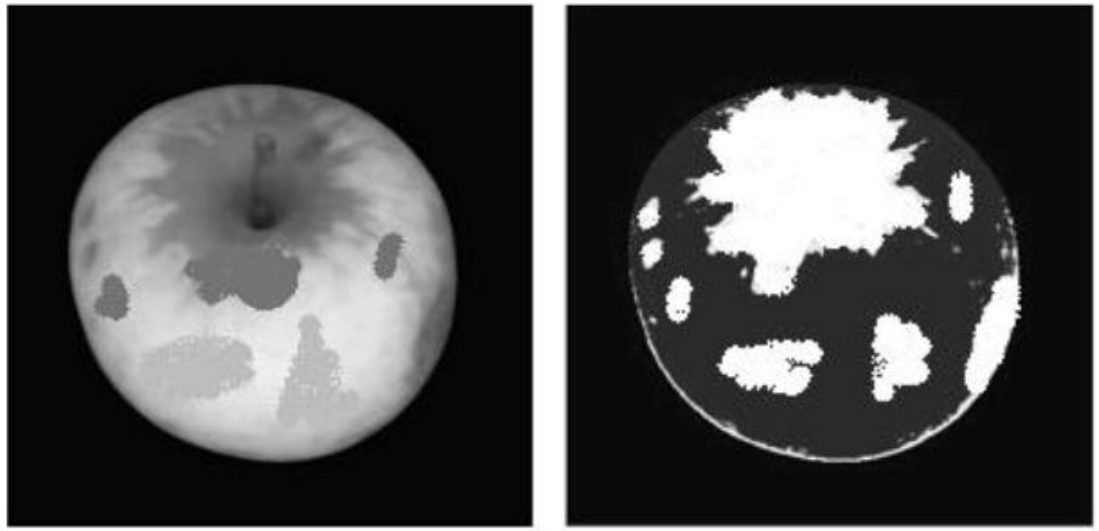

FIGURE 4.13
Surface inspection—image of an apple and the processed output.

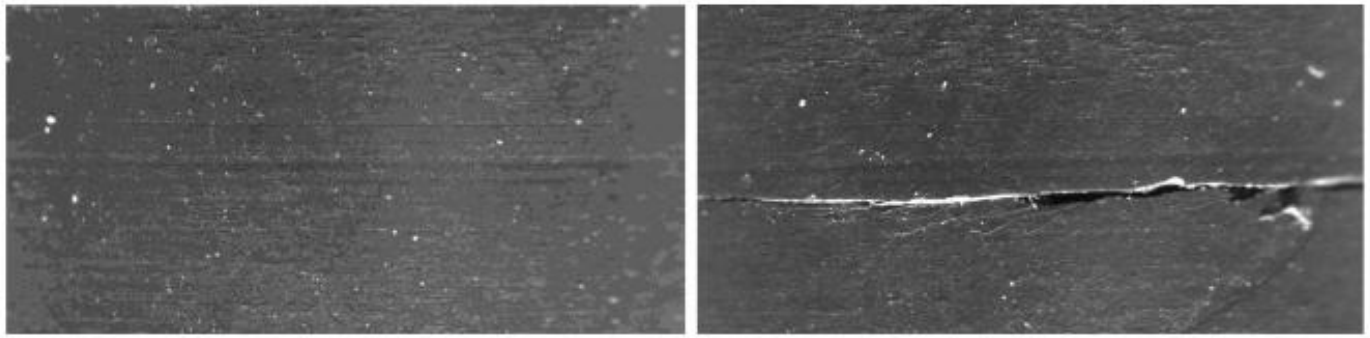

FIGURE 4.14
Surface inspection—image of a tyre and its processed output.

Anand, Sheila & Loganathan, Priya. (2019). A Guide for Machine Vision in Quality Control.

Categorization of Machine Vision Solutions

Robotic guidance

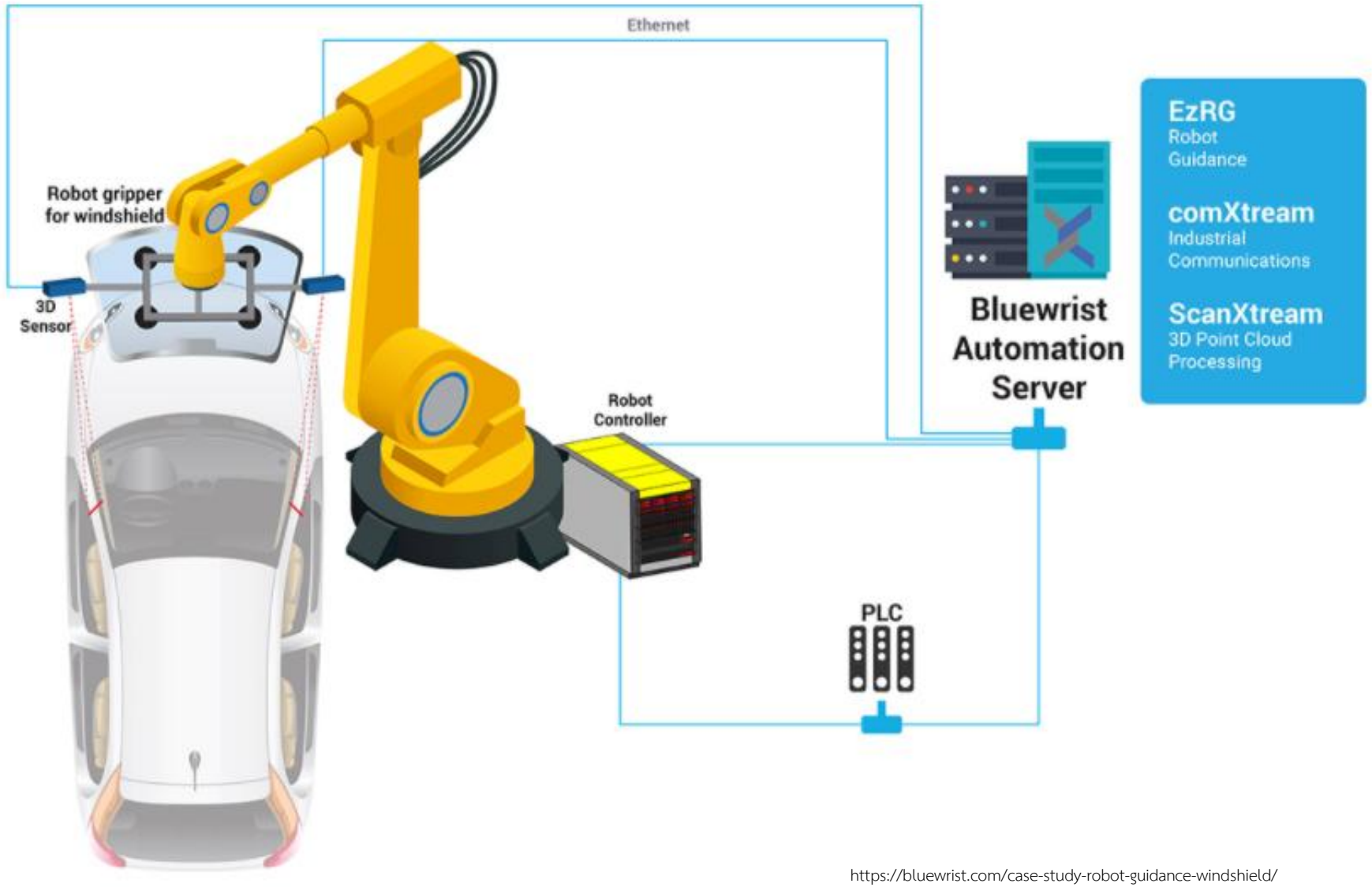

https://bluewrist.com/case-study-robot-guidance-windshield/

General Process for Building Machine Vision Solutions

Some of the questions that need to be asked to arrive at the requirements of the application:

- Is the part a discrete object or is it continuous (paper or cloth)?
- Can the part be momentarily stationery for image capture, or will it be continuously moving?
- Is the shape of the object regular or irregular?
- What type of inspection needs to be carried out?
- What features of the part need to be extracted?
- What type of image processing methodology is best suited to the application?
- Is it monochrome or color image processing?
- Will the parts be separate or will they overlap?
- What are the timing requirements?
- What are the other performance requirements?

Case Study: Presence/Absence Inspection of a 3G Switch Box

The quality inspection needs to check

1. Front of the box
- Presence/absence of connector covers

2. Back of the box
- Presence/absence of fan
- Presence/absence of warning label
- Presence/absence of barcode

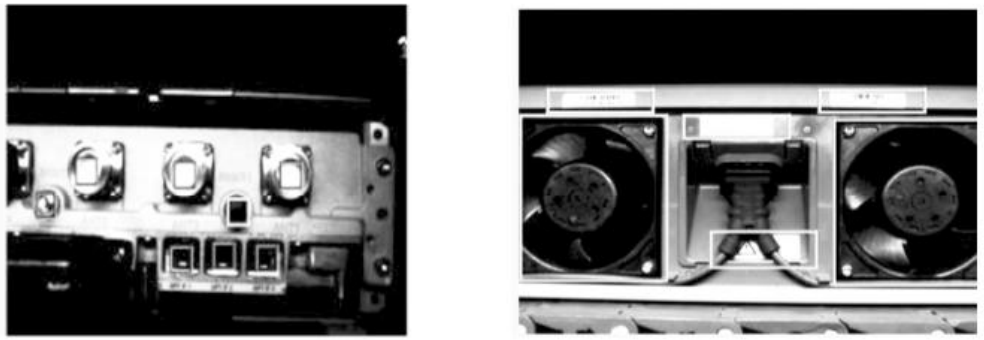

FIGURE 6.1
3G switch box (front and back views)—case study

The length of the switch box is 15 mm. if the camera sensor is 36 mm wide and 24 mm high, its aspect ratio would be 3:2. Let us assume an aspect ratio of 4:3 as most compact cameras come in this size. FOV is calculated in the vertical and horizontal directions as follows:

$$FOV_{ver} = Maximum\ part\ size\ +\ Tolerance\ in\ positioning\ +\ Margin = 15 + 1 + 1 = 17\ mm$$

$$FOV_{hor} = FOV_{ver} \times \frac{4}{3} = 17 \times \frac{4}{3} = 22.66\ mm$$

The field of view is therefore 17 × 22.66 mm.

Anand, Sheila & Loganathan, Priya. (2019). A Guide for Machine Vision in Quality Control.

Case Study: Presence/Absence Inspection of a 3G Switch Box

The resolution of the camera
we define spatial resolution as number of pixel values per millimeter. In other words, it is the number of pixels mapped to the smallest size that is to be measured. Let the smallest detail Sd be measured to be 0.1 mm for our case study. This is largely based on the measurement accuracy that is required. Let us map 1 pixel for the smallest detail. Then,

$$R_s = \frac{Smallest\ detail\ to\ be\ measured}{Number\ of\ pixels\ to\ map\ the\ smallest\ details} = S_d/N_s = 0.1/1$$

$$R_{hor} = FOV_{hor}/R_s = 22.66/(0.1/1) = 226\ pixels$$

$$R_{ver} = FOV_{ver}/R_s = 17/(0.1/1) = 170\ pixels$$

The camera with a resolution of 480 × 240 mm. => A standard 1 megapixel (MP) camera can be chosen for our application. Horizontal field of view can be used to decide the focal length. A normal lens of focal length greater than 22.6 mm obtained through the FOV calculation can be used. Lens size is of 5, 13, 15, 17, 20, 25 mm, etc. Since the nearest higher lens size is 25 mm, it is better to opt for a standard lens size of 25 mm.

Anand, Sheila & Loganathan, Priya. (2019). A Guide for Machine Vision in Quality Control.

Case Study: Surface Inspection of a Rivet

Let the size of the rivet be 5 mm. Let the surface smoothness of the rivet be measured with an accuracy of 0.1 mm. Let the time frame for processing be 2.5 seconds. The requirement in this case study is to inspect the surface for smoothness. Surface discontinuities like burrs or scratches should not be present. Blob analysis can be chosen as an appropriate technique for image analysis.

For this case study, we assume the aspect ratio is 5:3, which is another standard aspect ratio in cameras. FOV is calculated in the vertical and horizontal directions as follows:

$$FOV_{ver} = Maximum\ part\ size\ +\ Tolerance\ in\ positioning\ +\ Margin = 5 + 1 + 1 = 7\ mm$$

$$FOV_{hor} = FOV_{ver} \times \frac{5}{3} = 7 \times \frac{5}{3} = 11.66\ mm$$

The field of view is therefore 7 × 11.66 mm.
The FOV was computed as 11.66 mm in the horizontal direction; hence, a lens with a FOV of 12.5 mm can be chosen. The working distance between the camera and the object can be adjusted to obtain an image of good clarity.

Anand, Sheila & Loganathan, Priya. (2019). A Guide for Machine Vision in Quality Control.

Case Study: Surface Inspection of a Rivet

As the FOV and the accuracy of the measurement are known, the necessary sensor resolution can be calculated as before:

$$R_c = \frac{FOV}{R_s} = FOV \times \frac{N_d}{S_d}$$

The requirement specification is for an accuracy of 0.1 mm and we will map 1 pixel for the smallest detail. The horizontal and vertical resolutions can be evaluated as:

$$R_{chor} = 7\ mm \times \frac{1\ pixel}{0.1\ mm} = 70\ pixels$$

$$R_{cver} = 11.6\ mm \times \frac{1\ pixel}{0.1\ mm} = 116.6\ pixels$$

The camera with a resolution of 70 × 116.6 pixels.

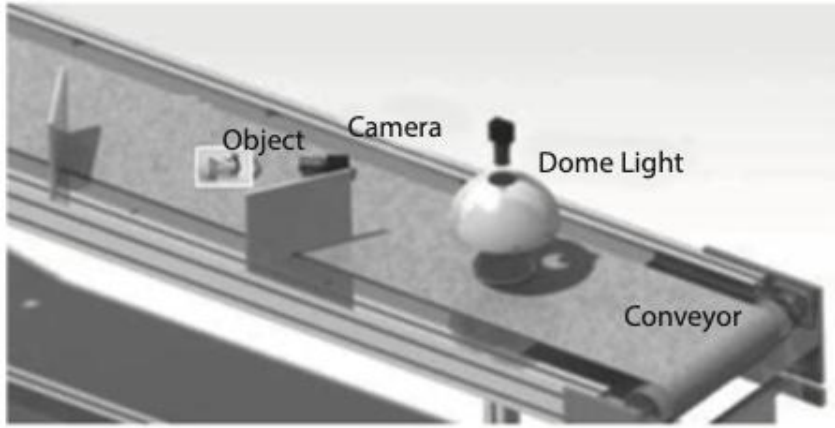

Anand, Sheila & Loganathan, Priya. (2019). A Guide for Machine Vision in Quality Control.

Case Study #3 : Gear-tooth Inspection

In industrial machine vision, how a watch gear could be inspected to check whether it had any missing or broken teeth. The inspection gear-tooth has maximum measurement of 7 mm and minimum defect size of 0.005 mm should be detected. Tolerance and margin will be fixed for 1 mm. The aspect ratio of the camera be 4:3.

1. Determine the camera resolution and FOV. Camera should have enough resolution to have at least 3 pixels for minimum defect size.
2. Find the location of missing or broken teeth by using OpenCV.

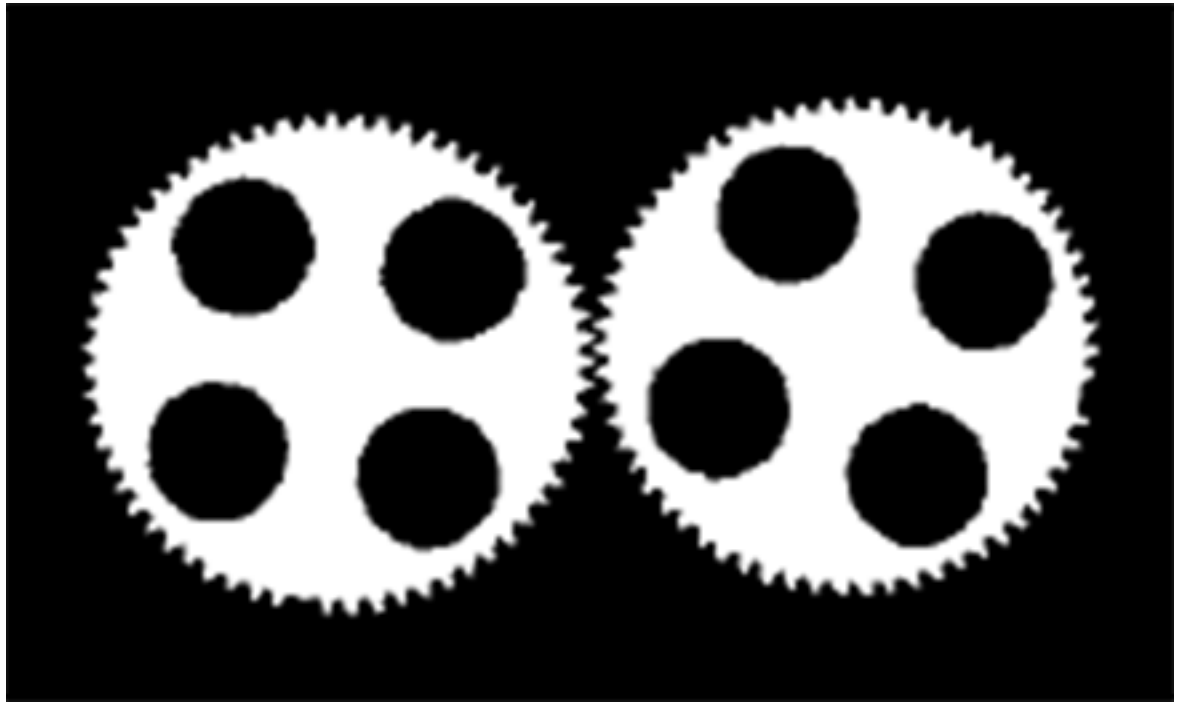

Sternberg (1985)